Phase Diagram of a Driven Lattice Gas of Two Species with Attractive Interactions

Edward Lyman

Virginia Polytechnic Institute and State University

A dissertation submitted in partial fulfillment of the degree of

Doctor of Philosophy in Physics.

Beate Schmittmann, chair
William Ducker
Guy Indebetouw
Uwe Täuber
Royce Zia

Department of Physics, Robeson Hall,
Blacksburg, VA 24060
April, 2004

Keywords: Driven lattice gas, Monte Carlo simulation, nonequilibrium phase transition

Phase Diagram of a Driven Lattice Gas of Two Species with Attractive Interactions

Edward Lyman

Abstract

We study the phase diagram of an interacting lattice gas of two species of particles and holes, driven out of equilibrium by a local hopping bias (denoted by 'E'). Particles interact by excluded volume and nearest-neighbor attractions. We present a detailed Monte Carlo investigation of the phase diagram. Three phases are found, with a homogenous phase at high temperatures and two distinct ordered phases at lower temperatures. Which ordered phase is observed depends on the parameter f, which controls the ratio of the two types of particles. At small f, there is nearly a single species, and a transition is observed into a KLS-type ordered phase[1]. At larger f, the minority species are sufficiently dense to form a transverse blockage, and a sequence of two transitions are observed as the temperature is lowered. First, a continuous boundary is crossed into an SHZ-type ordered phase[2], then at a lower temperature a first-order boundary is crossed into the KLS-type ordered phase. At some critical value of f is a bicritical point, where the first-order line branches from the two continuous boundaries. We also consider correlations in the homogenous phase, by constructing a continuum description and comparing to the results of simulations. Long range correlations are present in both the theoretical results and the simulations, though certain details of the theory do not fit the observations very well. Finally, we examine the beahvior of three-point correlations in the single-species (KLS) limit. Nontrivial three-point correlations are directly related to the nonzero bias E. We therefore consider the behavior of the three-point correlations as a function of E. We find that the three-point signal saturates very rapidly with E. There are some difficulties interpreting the data at small E.

Acknowledgements

Since I have arrived at Virginia Tech, I have benefitted greatly from the collaboration and protection of Beate Schmittmann, Uwe Täuber, and Royce Zia. I should especially like to thank my advisor Beate for all our discussions, all her advice, and most of all, her apparently unlimited patience. Without that patience, I never would have made it. Thanks to Royce for our very first conversation, which convinced me that there were good people doing interesting research at Virginia Tech. Since then, his support has been invaluable. Thanks to Uwe for taking the time to teach some great courses to a handful of students. When I find myself in front of the class, I will strive to match his high standard. I have also benefitted from other members of the group, past and present. Especially Robert Astalos, whose help likely saved a month of testing when I first developed my code. And Ivan Georgiev, who passed along some crucial pieces of code and other technical expertise. His work is in this dissertation, in the snapshots and animations of the model.

There are other people in the department who have smoothed many wrinkles. Chris Thomas, who has likely been mentioned in every thesis and dissertation since her arrival here. Roger Link, who never let on that my technical questions belied a terrible naïveté. And Judy Faw, our buffer from the bureauocracy.

If I had thanked people in chronological order, I should have begun with my parents. Against the advice of their friends, who cautioned that their economic situation did not recommend a second child, they went ahead and had a second child anyway (Thanks!). Next I should have thanked Ajay Mehra, who pushed me to continue my studies at a critical moment. I remember well the circumstances of that conversation, and I remain thankful for his friendship.

Contents

List of Figures

Chapter 1

Introduction

1.1 Equilibrium Redux

When we say that a lump of matter is *in equilibrium*, we have in mind a set of assumptions. In words, we are saying that this lump is somehow isolated from the world, so that it exchanges no matter or energy with the rest of the world. It just sits there, nothing (macroscopic) happens, and nothing (macroscopic) changes. Strictly speaking, such an idealization is fictitious, though in many cases this approximate description is more than good enough. (And quite interesting in many cases.) However, in this work we are interested in situations where this assumption is not good enough. All living things fall into this latter category: energy flows through in order to maintain a high level of organization. But before we can turn to these natural problems in all their complexity, we need to develop some techniques and principles to guide our investigations, lest we become hopelessly entangled by the details. That is the subject of this dissertation.

Simple models have a long and illustrious history in the development of statistical methods for physical systems. In the 19^{th} century, the ideal gas model lent organization and physical meaning to the investigations of Maxwell, Boltzmann, Gibbs and others[3]. Their investigations led to the formulation of a unified structure for the treatment of equilibrium models, about which we will say more below. In the early 20^{th} century, Lenz and Ising[4] introduced a simple model for magnetism, which was originally derided as overly simplistic[5]. Besides being useful for theoretical development as a minimal model for *interacting* systems, the Ising model does in

fact describe magnetism in some materials. (For a brief review and further references, see[6].)

We should therefore not be too quick to dismiss a model as 'too simple,' often the insight gained will survive multiple layers of complexity. Thanks in large part to the study of these models, we have at our disposal a robust theoretical apparatus, which allows a theoretical treatment of any equilibrium model[7]. Here we review the fundamental parts of this apparatus, so as to contrast it with the situation for nonequilibrium models.

We are able to compute various observables (e.g., average density, correlation functions) for equilibrium models, because we know precisely the distribution which describes the likelihood that the model is found in a particular configuration. To be specific, the probability $P^{eq}(C)$ to take a configuration C with Hamiltonian H_C is given by the Boltzmann distribution:

$$P^{eq}(C) = \frac{e^{-H_C/k_BT}}{\mathcal{Z}} \tag{1.1}$$

where the normalization factor $\mathcal{Z}$ is called the partition function and is computed by summing the weight of each configuration over all possible configurations:

$$\mathcal{Z} = \sum_{\{C\}} e^{-H_C/k_BT} \tag{1.2}$$

The system is assumed to be in contact with a heat bath at a temperature T; multiplying T by Boltzmann's constant k_B gives the energy scale of thermal fluctuations. By taking appropriate derivatives of $\mathcal{Z}$ we can compute, e.g., the average energy: $\langle E \rangle = -\partial \ln \mathcal{Z}/\partial\beta$, where β is a shorthand for $1/k_BT$. In contrast, we do not know what $P(C)$ looks like for nonequilibrium systems; in the most general case it will depend on time as well. Even in cases when we have a *stationary* distribution for our far from equilibrium model (which we will refer to as $P^*(C)$), that distribution will not necessarily be the Boltzmann distribution: $\lim_{t\to\infty} P(C,t) = P^*(C) \neq P^{eq}(C)$. Our focus here will be on models which *are* described by a stationary distribution, but for which that distribution is *not* $P^{eq}(C)$.

1.2 Monte Carlo Simulation

Even though we do not know in general the shape of distributions for nonequilibrium systems, we can always write the master equation for the distribution:

$$\partial_t P(C,t) = \sum_{C'} \{W[C' \to C] P(C',t) - W[C \to C'] P(C,t)\} \tag{1.3}$$

where $W[C' \to C]$ is the rate (probability/unit time) to go from configuration C' into C. The master equation is an equation of motion for the probability; the terms on the right are currents of probability into and out of $P(C,t)$. For stationary distributions, the long-time limit of eq. (1.3) yields a relationship between the rates W and the distribution P:

$$0 = \sum_{C'} \{W[C' \to C] P(C') - W[C \to C'] P(C)\} \tag{1.4}$$

Though we can rarely solve this equation exactly[1], the master equation suggests a general way to build computer models. For example, a configuration may be a particular arrangement of Ising spins on a lattice; at each lattice site a variable takes the value $+(-)1$ for an up(down) spin. A site is chosen at random and updated according to the rates W: in our example, a spin is flipped or not depending on its neighbors, external fields, etc. By repeating the procedure many times, a sequence of configurations is generated. This sequence samples the distribution $P(C,t)$, and eventually $P(C)$ once the system reaches the stationary state. This technique, called *Monte Carlo simulation*[2] for the way it randomly samples a distribution, was originally developed for numerical studies of equilibrium systems. Of course, which $P(C)$ is sampled depends on the W's, as well as boundary conditions and other constraints. If we should wish $P(C)$ to be $P^{eq}(C)$, then a very strict condition is imposed on the rates. This condition, called *detailed balance*, demands that for any closed loop of configurations, the product of rates to

[1] One would have to diagonalize an $N \times N$ matrix, where N is the number of configurations. For a one dimensional chain of n Ising spins, $N = 2^n$. Diagonalization of a $2^n \times 2^n$ matrix requires approximately $2^{n \log_2 7}$ operations, which is unfeasible even for modest n

[2] Actually, what we have just described is a particular type of Monte Carlo sampling, called importance sampling. By virtue of its trajectory through phase space, this sort of algorithm draws most of its configurations from the most likely region of the distribution. It thus outperforms a truly random sampling, which would spend an unnecessarily long time attempting to sample the thin tails of the distribution.

go one way around the loop must equal the product in the reverse order[8]. This must hold for *all* loops. Thus, for any pair of configurations we have:

$$\frac{W\left[C' \to C\right]}{W\left[C \to C'\right]} = e^{-(H_C - H_{C'})/k_B T} \tag{1.5}$$

where for $P(C)$ we have substituted the Boltzmann distribution, (eq. 1.1). If we wish to simulate an equilibrium system, we are free to choose the W's however we like, so long as they fulfill condition 1.5. Indeed, some W's may perform better than others under certain circumstances, and a judicious choice may save valuable computer time[9]. This is in contrast with the situation away from equilibrium, where properties of the stationary state may depend on the details of the rates[10]. It remains an open question which parts of the rates 'matter', and which do not. Until this is known, one cannot arbitrarily select a new rate in the interest of saving computer time, for it may be that this new rate defines a new model.

Indeed, this practical issue raises an issue of general theoretical interest regarding nonequilibrium models. Near an equilibrium critical point, universal behavior is observed. By universal, we mean that several distinct microscopic models are mapped onto the same mesoscopic model, on the basis of symmetries and conservation laws[11]. In the critical region, three independent exponents suffice to describe the behavior of measurable quantities. This is quite powerful, for by studying the simplest model in a particular universality class we can compute quantities relevant for the most complex. It is yet unclear whether such a classification scheme will turn out to be useful for phase transitions far from equilibrium. Not only must symmetries and conservation laws be accounted for, but also the dynamics. To date, only *nonuniversal* quantities have been found to depend on the choice of dynamics[10]. Indeed, the 'model A' universality class is remarkably robust against all manner of perturbations[12], and the directed percolation class appears in many different contexts[13]. In this work, these issues will be discussed in the context of our particular model.

The remainder of the dissertation is organized as follows. We continue the introduction by reviewing the literature relevant to the present work. This will provide both some historical background and a context for our own investigation. We then discuss our model in detail and define the quantities which were measured. Computational results follow, and then a summary and discussion of open questions.

1.3 Driven Diffusive Models – A Brief Review

1.3.1 One-dimensional models

Even in one dimension, nonequilibrium systems are capable of very interesting behavior. Roughly, this is because we have available an extra dimension, since the system is evolving in time. In fact, there is a formal analogy between the dynamics of a $1+1$ dimensional stochastic process and the equilibrium statistical mechanics of a 2 dimensional system[14]. We should therefore not be surprised to see, e.g., spontaneous symmetry breaking in $1D$ nonequilibrium systems with short-ranged interactions, as such transitions are known to exist in $2D$ equilibrium systems. Consider, for example, a single species of particles, interacting only through excluded volume and with a simple biased-diffusion dynamics, the asymmetric exclusion process or ASEP. An exact solution is available for a periodic lattice; there is one phase which is a homogenous distribution of particles. (This result holds for any dimension[15].) If we consider instead open boundary conditions, parameterized by the injection rate of particles at one end and the removal at the other, the model is again exactly solvable[16]. Now a rich phase diagram emerges, with a high density phase, a low density phase, and a phase which maximizes the particle current.

The observed phases are controlled by the injection and removal rates. This *boundary-induced phase transition* is made possible by the current, which transmits the effects of the boundaries into the bulk. Contrast this with the situation in equilibrium, where, in the absence of currents, long-ranged interactions would be necessary to observe such a transition. In the ASEP no such long-range interactions are built into the model, rather they are dynamically generated by the asymmetric dynamics and the (bulk) conservation law. Beyond the theoretical interest, related models have been studied as a possible description of the motion of a ribosome along an mRNA molecule[17].

One can consider generalizing the above single-species model to two species which are biased to hop in opposite directions. Of course, the excluded volume constraint must be softened in order to render the system ergodic. In this case, the periodic system again is again disordered, though now the steady-state is nontrivial, consisting of small clusters with an exponential

distribution in the cluster size[18]. Such models have been considered as simple models of traffic flow, where the two species of particles are (in the co-moving frame) fast and slow vehicles. Though there is no phase transition in the strictly $1D$ system, something interesting happens when a 'two lane' or quasi $1D$ system is considered. Simulations show the appearance of a single macroscopic cluster[19]. This behavior is at odds with our intuition, which suggests that in the thermodynamic limit the quasi $1D$ system should behave as the strictly $1D$ system. Recently, some authors have suggested that the effect is a manifestation of a subtle finite-size effect, in which the quasi $1D$ system crosses over to strictly $1D$ behavior only for very large systems, on the order of 10^{70} lattice sites[20]. Though the debate awaits a resolution, we see in either case that a rigorous treatment of phase transitions far from equilibrium can be a subtle, tricky affair. This is a theme which we will encounter again in this work, and is worth remembering as a rule-of-thumb for nonequilibrium systems.

1.3.2 Two-dimensional models

We now consider models in $d > 1$. As mentioned above, the biased diffusion of a *single* species on a periodic lattice, interacting only through excluded volume, has a single phase of homogenous density. By introducing nearest-neighbor attractive interactions, Katz *et al.* ('KLS') hoped to understand the physics of fast ionic conductors[1], as well as develop a nontrivial model for basic investigations. As a single parameter (the hopping bias) modification of the Ising lattice gas, the KLS model is a *minimal model* for the study of nonequilibrium steady states (NESS). Particle hops along one direction (parallel to the x-axis) occur at the normal equilibrium rate, as if in contact with a heat bath at temperature T. Particle hops in the other direction (parallel to the y-axis) are enhanced (suppressed) in the positive (negative) direction by coupling to a hopping bias, E. With periodic boundaries in the y-direction, a nonzero current is maintained, and the system settles into a NESS. At half-filling, there exists a continuous transition, though with $T_c(E)$ increasing monotonically with E and saturating at $1.414T_c(E = 0)$[21],[22],[23]. The transition falls into a novel universality class with exponents distinct from the Ising ones[24]. The critical behavior is strongly anisotropic, with distinct sets of exponents characterizing fluctuations *perpendicular* and *parallel* to E. There has been some discussion regarding the nature of these fluctuations, with some authors disputing the original claim that the correct meso-

scopic description is gaussian in the perpendicular direction[25]. Though the anisotropy makes numerical investigation of the critical behavior quite subtle and computationally intensive, recent high precision Monte Carlo studies compare the two mesoscopic descriptions. The results are in complete agreement with the predictions of the original field theory[21]. As a final note, we mention that the combination of anisotropic dynamics and a conservation law introduces power law correlations at all $T > T_c$[26], a manifestation of the relaxation of the detailed balance constraint. These correlations are revealed by the structure factor, which has a discontinuity singularity at the origin. In this sense, even the 'disordered' phase is quite non-trivial.

Turning to multispecies versions, the simplest ('SHZ') model[2] allows *two* different types of particles, distinguished only by their interaction with the external field. Positive (negative) particles are biased to hop in the positive (negative) y-direction, and interact only via an excluded volume constraint. (The attractive interactions are neglected in a first approximation, where we take E and $T >> J$, with E/T fixed.) The temperature is absorbed into E and the only parameters are E, the overall mass density m, and the overall charge density (i.e., the density difference of the two species), f. Here, the mechanism for ordering is the mutual volume exclusion of the particles, so that at sufficiently strong E and large m, the system locks into a high density strip *perpendicular* to E, with positive and negative particles blocking each other. Note the contrast with the situation discussed above, where, in $D = 1$, there is no phase transition. For non-zero charge density f, this strip is found to drift in the direction of the minority species[27]. Depending on where the phase boundary is crossed, first-order or continuous transitions are observed[28],[29]. Various other remarkable properties have been discovered. For a range of aspect ratios, configurations with non-zero winding number ('barber poles') are quite frequently observed, *in addition* to the usual transverse strips, raising the possibility of bistability[30]. As in the KLS model, power law correlations characterize the disordered phase, now with *directionality-dependent* exponents[31]. In this work, we will return to the question of long-range correlations in the 'disordered' phase.

In this dissertation, we consider the two-species model at finite T and E, where interparticle interactions are expected to play an important role. By varying T, E, and f, the fraction of the *total* population which are of the *minority* species, we can interpolate smoothly from the KLS model to the (non-interacting) two-species SHZ model. Hence, we expect a competition between the two types of ordered configurations – parallel vs transverse strips

– favored by these two limits. As f varies from 0.0 (KLS model) to 0.5 (equal numbers of each), there should be some critical f where the preferred order switches. To explore these phenomena in more detail, we map out the phase diagram in E, f and T, for a range of system sizes. The energy scale is set by our choice of the interparticle attraction J, and the overall mass density m is fixed at 0.5 so that the Ising critical point remains accessible. Many questions arise in connection with earlier work. How does the presence of nearest neighbor attractions modify the two-species transition? What will be the effect of a few 'impurities' (i.e., minority particles) on the KLS transition? At what concentration do the 'impurities' become relevant and change the nature of the transition? We will be able, if not to answer these questions fully, then to at least suggest the character of their resolution sufficiently to guide further research.

In the next chapter we present the phase diagram of the two-species model in the parameters f, E, and T, as mapped by Monte Carlo simulation. In the following chapter we develop an analytic description of the homogenous phase, and then compare the predictions of the theory to simulation results. We aim to see which features are captured by the theory presented, and which may require some modification. We then discuss an interesting signature of nonequilibrium behavior in the KLS model, namely the three-point correlations which are generated by the bias. We conclude by summarizing our findings and discussing possibilities for future research.

Chapter 2

Phase Diagram

In this chapter, we present extensive numerical results for the phase diagram of the interacting two-species model. Our main results are as follows. At fixed E and sufficiently small f, a line of continuous transitions emerges from the pure KLS ($f = 0.0$) point. Upon crossing this line, the disordered phase becomes unstable and orders into a strip parallel to E. As we increase f, we encounter a bicritical point, where the line of transitions bifurcates, into a line of continuous order-disorder transitions into a strip transverse to E, and a line of first-order transitions along which transverse and parallel order coexist. If we fix f and lower T, we first observe the transition from disorder into the transverse strip, followed by a transition into parallel order. This topology persists at higher E, except that all lines are shifted to slightly higher temperatures. The size-dependence of the phase diagram is subtle, since the main features are controlled by *different* scaling variables. On the one hand, the transition into the transverse strip is controlled by the *effective* drive $L_y E/T$ where L_y is the system size in the drive direction. On the other hand, the bicritical point appears to depend on the scaling variable $L_y f$ which translates into the number of *rows* (transverse to E) which can be filled with the minority species. Finally, the pure KLS point requires finite-size scaling at fixed shape factor $A \equiv L_y^{\nu_\perp/\nu_\parallel} L_x^{-1}$[22], in two spatial dimensions.

The remainder of the chapter is organized as follows. We first describe in detail the microscopic model and the observables which are used to locate the different phases. We then present our simulation results, beginning with the structure of typical configurations in different parts of parameter space and of their associated order parameters. By monitoring the signatures of first and

second order transitions, we compile a cut through the phase diagram at fixed E, with variable f and T. The phase boundaries and their dependence on system size are analyzed in some detail. To complete the picture, we present two cuts at different but fixed temperatures, crossing the phase boundaries by varying E and f. We conclude with a brief summary and a discussion of some open questions.

2.1 Microscopic Model and Observables.

We consider periodic square lattices of size $L_x \times L_y$, in two spatial dimensions, with E parallel to L_y. A configuration is specified by the set of occupation variables, $\{\sigma(\mathbf{r})\}$, where $\sigma(\mathbf{r})$ takes three values, $\pm 1, 0$ denoting a positive (negative) particle, or hole at lattice site $\mathbf{r}$. Often, we will only need to distinguish particles from holes, via $n(\mathbf{r}) \equiv |\sigma(\mathbf{r})|$. All lattices are half filled, i.e., $m \equiv (L_x L_y)^{-1} \sum_{\mathbf{r}} n(\mathbf{r}) = 1/2$, so that the Ising critical point remains accessible. An important parameter is the fraction of negative particles (the 'minority species') in the system: $f = 2(mL_xL_y)^{-1} \sum_{\mathbf{r}} \delta_{-1,\sigma(\mathbf{r})}$. Clearly, we only need to consider the sector $0 \leq f \leq 0.5$, from having no negative particles at all to equal numbers of each species. For later reference, we also introduce the charge density, $Q \equiv (L_xL_y)^{-1} \sum_{\mathbf{r}} \sigma(\mathbf{r}) = m - f$.

The nearest-neighbor attraction is modelled by the Ising Hamiltonian

$$H = -4J \sum_{\langle \mathbf{r},\mathbf{r}' \rangle} n(\mathbf{r})\, n(\mathbf{r}') \tag{2.1}$$

We choose attractive interactions, $J > 0$, regardless of species. While many other choices are possible and interesting, ours provides maximum linkage to previously studied cases: Ising, KLS and SHZ. The Monte Carlo dynamics conserves the number of each species and is specified as follows. An update attempt begins by picking a bond at random. If the bond connects a particle-hole pair, the contents are exchanged with the Metropolis rate:
$\min\{1, \exp[-(\Delta H - \delta y E \sigma(\mathbf{r}))/T]\}$[33]. Hence, at $E = 0$ we recover the equilibrium Ising model with conserved magnetization, coupled to a heat bath at temperature T. We will set $J = 1$ and measure E in units of this (arbitrary) energy scale. The change in y-coordinate, due to the proposed move, is denoted by δy, and ΔH is the associated change in internal energy. The term $\delta y E \sigma(\mathbf{r})$ models the gain or loss of energy from the coupling to E; if $\delta y \sigma(\mathbf{r})$ is positive (negative) the move is favored (unfavored).

Our model, in which E and T are varied independently, raises an interesting issue. If the ratio E/T is quite large, it becomes almost impossible for particles to hop backwards. In a finite system, this implies that a relatively small fraction of the minority species – provided the 'right' fluctuation occurs – is sufficient to form a stable blockage. Even though such a fluctuation becomes less probable in a larger system, the dynamics nevertheless becomes nonergodic in the limit $E/T \to \infty$. In principle, this can be avoided by introducing, e.g., a small probability for particles to exchange places [29]. To limit the number of parameters, we circumvent these problems here by considering different initial configurations and a range of system sizes.

The dynamics is diffusive, and therefore conserves both charge and mass density. Though the *local* effect of the external field is analogous to the effect of an electrostatic potential on electric charges, the boundary conditions exclude the possibility of a *global* Hamiltonian description.

As overall density is conserved, we expect ordered configurations to be strips of higher density coexisting with strips of lower density. The structure factor,

$$S(m_x, m_y) \equiv \left\langle \left| \frac{\pi}{L_x L_y} \sum_{x,y} n(x,y) e^{2\pi i (m_x x/L_x + m_y y/L_y)} \right|^2 \right\rangle \qquad (2.2)$$

then serves as a good order parameter, since it is sensitive to *mass-segregated* strip configurations. It is labelled by (integer) wavenumbers,
$m_x, m_y = 0, 1, ..., L-1$. So, for example $S(1,0)$ will be $\mathcal{O}(1)$ for a strip aligned with the field, characteristic of KLS order; similarly, $S(0,1)$ will detect a strip transverse to E which develops in the SHZ (two-species) model; and both are normalized to $\mathcal{O}(1/L_x L_y)$ for a disordered configuration. We also monitor a 'susceptibility', i.e. the fluctuations of the order parameter:

$$\Delta(m_x, m_y) \equiv \left\langle S(m_x, m_y)^2 \right\rangle - \left\langle S(m_x, m_y) \right\rangle^2 \quad . \qquad (2.3)$$

We note that $S(m_x, m_y)$ is the Fourier transform of the *mass* variable, and therefore not sensitive to any charge-segregated structures. Replacing $n(x,y)$ by $\sigma(x,y)$ in Eq. (2.2) generates structure factors which respond to charge inhomogeneities. We have monitored these and their fluctuations throughout, and found that their behavior is consistent with the mass-based quantities.

When S is calculated, the average is taken over multiple steady-state configurations of a Monte Carlo run, with a typical run lasting $0.8M$ Monte

Carlo steps (MCS) and $2L_xL_y$ bond update attempts per MCS. Data are collected every 400 MCS; fluctuations of observables indicate that this interval is sufficient to produce uncorrelated data in the largest (60×80) systems considered. Typically the initial $0.2M$ MCS are discarded to ensure that data are taken from the steady state. Near critical points and at low temperatures these numbers require modification, due to long correlation times and long-lived metastable states. In such cases the only recourse is a painstaking analysis of individual, very long runs. When that is necessary we will measure a quantity closely related to S:

$$s(m_x, m_y) \equiv \left| \frac{\pi}{L_x L_y} \sum_{x,y} n(x,y) e^{2\pi i (m_x x/L_x + m_y y/L_y)} \right|^2 \tag{2.4}$$

which measures the type of order present in a *single* configuration. We can then track s for different m_x's and m_y's over the course of a run and see precisely how the averages are generated.

Finally, at each bond update we tally the quantity $\delta y \sigma(x,y)$, which is then averaged over a run to give the charge current j. However, it is not particularly illuminating to compare j for different values of the effective drive E/T. We are more interested in a quantity which is a property of the gross structure of the steady state, namely, the conductivity κ defined via $j = \kappa E/T$.

Now that we have described the various quantities which will be used to probe the behavior of our model, we turn to the presentation of the data.

2.2 Results

2.2.1 Phase diagram in f and T

In this section we seek the location and character of transitions by scanning in f and T at fixed drive E. We choose $E = 2.0$ since this intermediate value still allows for a significant fraction of backward jumps, thus avoiding the spurious metastable configurations discussed above. At the same time, it is large enough to induce measurable currents and other clear signatures of far-from-equilibrium behavior. The two order parameters $S(1,0)$ and $S(0,1)$ and their fluctuations are monitored in order to identify the different phases. Large peaks in their fluctuations, or the presence of hysteresis, are used as

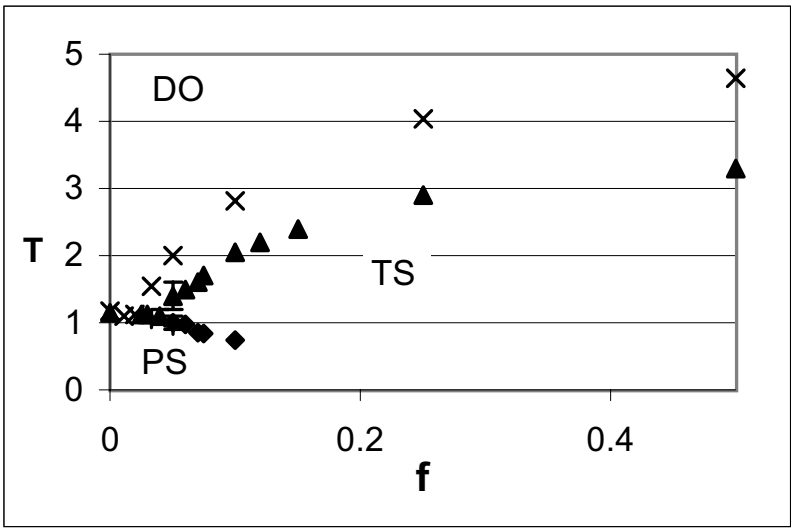

Figure 2.1: Phase diagram in f and T for $E = 2.0$. Triangles and diamonds are boundaries in the 40×40 system, $\times$'s are for the 60×60 system.

indicators of continuous vs first order transitions, respectively. For clarity, we first present a quick overview of the topology of the phase diagram, and then turn to the details of the data which underlie this picture. Figure 2.1 shows the phase diagram in the f-T plane, at $E = 2.0$, for two different system sizes. Three phases are found: a homogeneous, disordered phase (DO), a transverse strip (TS) phase as in the two-species model, and a parallel strip (PS) phase as in the KLS model. The value of f determines which phase is observed: at $f = 0.0$ there is only one species of particle, and a single transition is observed from disorder into the parallel strip. As f increases, this transition persists until the number of the minority species is sufficient to create a blockage and form the transverse strip. From here on, *two* transitions are observed: from disorder into the transverse strip, and at a lower temperature from the transverse strip into the parallel strip. Upon increasing f further, only the DO-TS transition can be detected. Although the TS-PS line cannot have a critical endpoint for reasons of symmetry, for $f > .10$ it occurs at such a low temperature that it cannot be observed in simulations of a reasonable length.

Now that we have briefly discussed the phase diagram we can look in more detail at the phases and their boundaries. Before presenting the data, (structure factors, their fluctuations, currents) we will begin with some pictures of typical configurations at various points in the phase diagram. This way the reader can develop some intuition about the model. All pictures

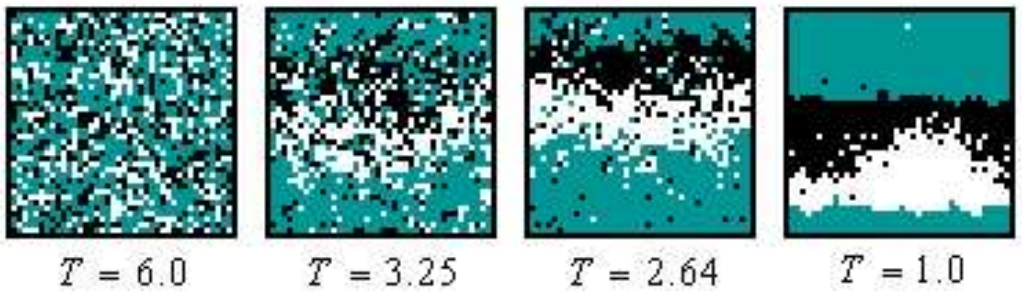

Figure 2.2: Configurations of the 40×40 lattice at $f = .50$ for four temperatures.

show 40×40 lattices, with E pointing up. White (black) pixels are positively (negatively) biased particles, light blue (gray in print) pixels are holes. Blue boxes in the electronic version are links to animations. We use a different color scheme in the animations: red(blue) pixels are $+(-)$ particles, black are holes. We will begin at the right side of the phase diagram and explore how typical configurations change as we move left, decreasing the fraction of the population which belongs to the minority species. In figure 2.2 we present four configurations at $f = .50$, or equal numbers of each type of particle. The first picture is at $T = 6.0$, well above $T_c = 3.3$. Unsurprisingly, this configuration lacks any visible structure since it falls deep in the homogeneous phase. This will be the only picture presented for the homogeneous phase, as the only *visible* feature which changes with f is the ratio of white

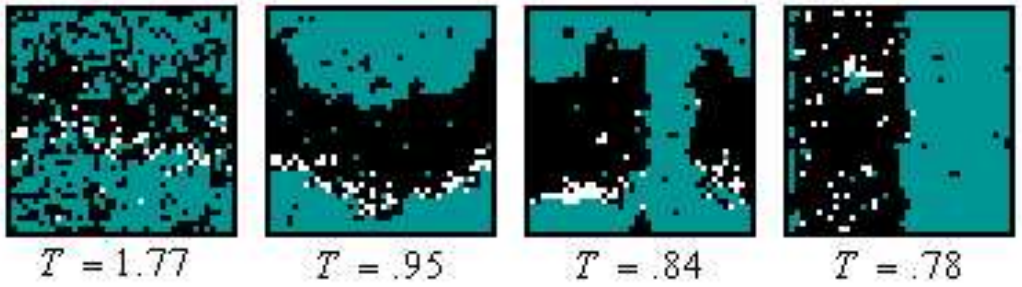

Figure 2.3: Configurations of the 40×40 lattice at $f = .075$ for four temperatures.

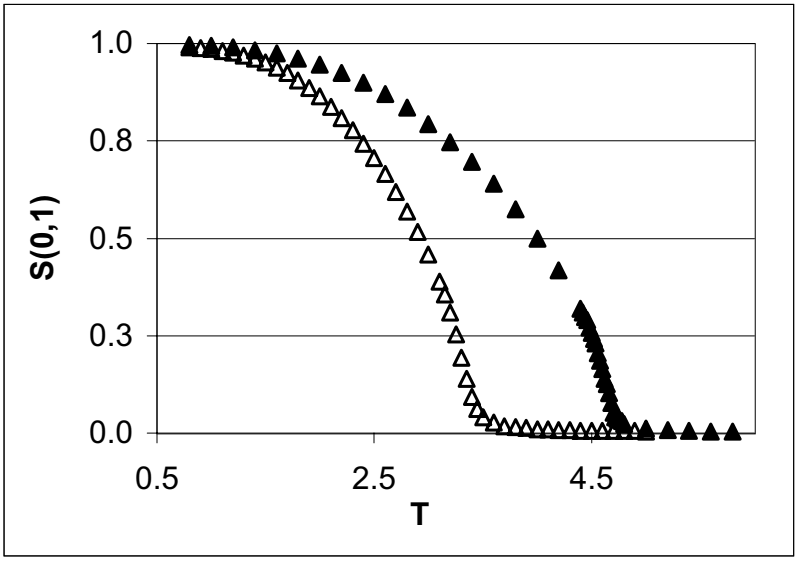

Figure 2.4: $S(0,1)$ as a function of T for $f = .50$. Open (filled) triangles are for the 40×40 (60×60) system.

to black pixels. The next picture is at $T = 3.25$, and now we begin to see the two-species type phase separation. Lowering the temperature further to $T = 2.64$, the horizontal strip appears quite clearly, though it remains diffuse at the boundaries, and there are many 'travelers' moving through the lower density region. At this temperature backward hops of particles are not too improbable, occuring with a rate $\exp(-E/T) = 0.47$, and thus a fair number of holes are able to enter the strip and allow for particles to slip through the blockage. Finally at $T = 1.0$ we are deep in the ordered phase, and now the boundaries of the strip become very sharp and travelers are few. At this temperature, holes are rarely able to penetrate into the interior of the strip. The irregular shape of the interface between the two species is a result of the quench from disorder; a more gradual lowering of the temperature would result in a smoother interface.

Lowering f further to .075 (Fig. 2.3) there are only 1.5 rows of the minority species. The first frame shows a configuration just below criticality at $T = 1.77$. Though they are still sufficient to form a blockage, the strip is no longer symmetric with respect to + and −. This leads to a drifting of the strip, as shown in the third frame. Occasionally, the rather thin blockage of the minority species is opened by backward hops, and the majority species

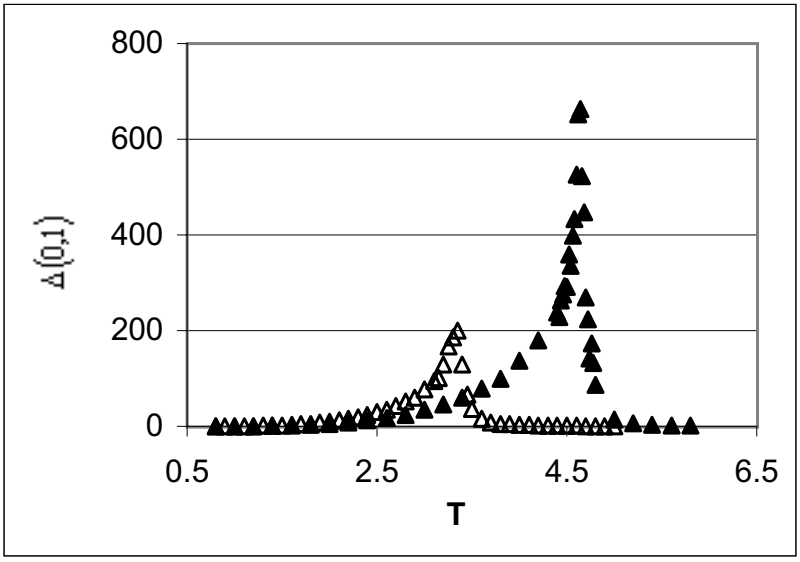

Figure 2.5: $\Delta(0,1)$ as a function of T for $f = .50$. Open (filled) triangles are for the 40×40 (60×60) system.

pours through. These majority particles are pushed around the periodic lattice and added onto the back of the majority blockage, leading to an upward drfiting of the strip. Lowering T further to .84 (third frame) it appears that interfaces *parallel* to E are becoming favorable; this sort of configuration is common at these intermediate values of f: here, parallel and transverse strips compete with each other. Indeed the final frame ($T = .78$) shows the preferred low temperature configuration: a single strip of *mixed* charge parallel to E, raising the possibility of a sequence of *two* transitions as a function of T.

Phase Boundaries

Now that we have developed a qualitative notion of the various regions in the phase diagram, we turn to a more quantitative analysis of the phases and their boundaries. As in the preceding section, we present the order parameters and their fluctuations as a function of T, for a range of f, though with one important difference: we will show data for at least *two* system sizes. While this cannot replace a high-precision finite-size scaling analysis of the transitions, it is intended to provide a rough picture of how the fluctuations

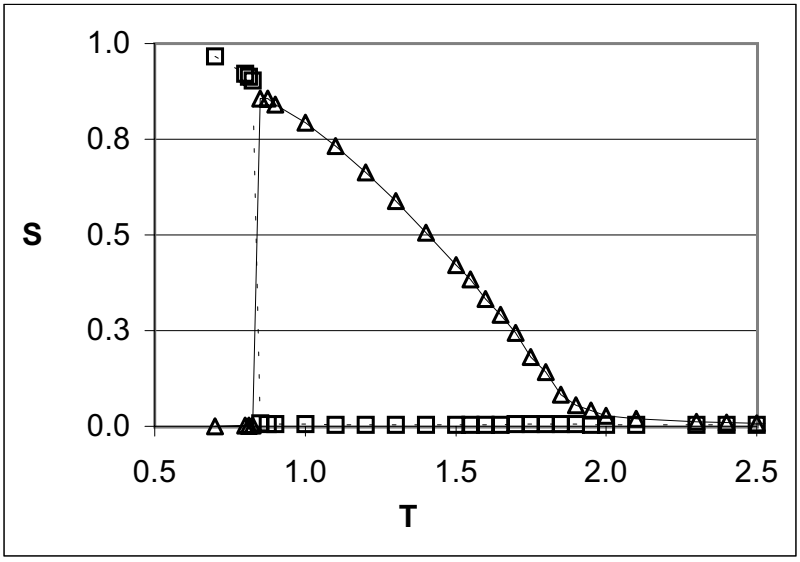

Figure 2.6: $S(0,1)$ and $S(1,0)$ as a function of T for $f = .075$ in the 40×40 system. Solid line with triangles (dashed line with squares) is for $S(0,1)$ ($S(1,0)$).

of the order parameter scale with system size.

We begin as before at $f = .50$, with equal numbers of each type of particle. In figures 2.4 and 2.5 $S(0,1)$ and its fluctuations are plotted as a function of T for the two system sizes; $S(1,0)$ is not shown as the only transition here is from the homogenous phase into the transverse strip. In both systems $S(0,1)$ goes smoothly to zero as T is increased (the inset shows the behavior for small T). A clean peak in $\Delta(0,1)$ is also observed in each system, increasing in amplitude with the system size. These two observations are consistent with a continuous transition into the transverse strip at $f = .50$, and we therefore use the location of the peak in $\Delta(0,1)$ to locate the phase boundary in figure 2.1, with $T_c(L = 40) = 3.35$ and $T_c(L = 60) = 4.64$.

Reducing f to a few rows of the minority species introduces some new features into the data, which we pause to briefly describe before continuing our analysis. At just a few rows of the minority species, we still observe the transition described above, with the same behavior of $S(0,1)$ and $\Delta(0,1)$. However, now that the strip is no longer symmetric we observe the drifting behavior described above. The ordered phase therefore fluctuates significantly, and $\Delta(0,1)$ develops a shoulder at about 1/3 the value it reaches at

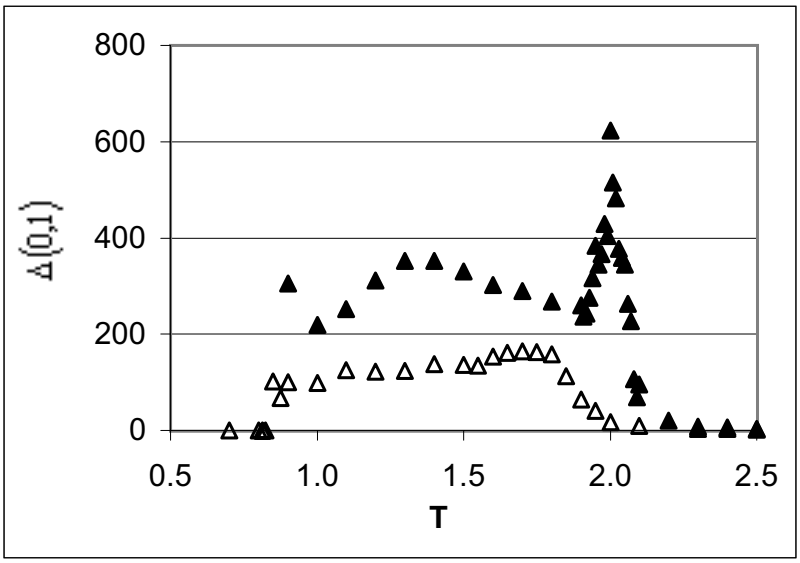

Figure 2.7: $\Delta(0,1)$ as a function of T for $f = .075$. Open (filled) triangles are for the 40×40 (60×60)system.

the transition. We will see below that the fluctuations of the ordered phase can obscure the transition in smaller systems.

Upon reducing f further we observe a sequence of *two transitions* as a function of T. Figure 2.6 shows both order parameters, $S(0,1)$ and $S(1,0)$ for 1.5 rows of the minority species: $f = .075$ in the 40×40 system. Also shown in figure 2.7 is $\Delta(0,1)$ for 1.5 rows of the minority species in both the 40×40 and the 60×60 system. We have omitted the 60×60 data for the order parameters to keep the plot clean; the behavior is similiar to that shown in the 40×40 system. As before, $S(0,1)$ and $\Delta(0,1)$ signal a continuous transition into the transverse strip as T is lowered, though the signal in $\Delta(0,1)$ is much more pronounced in the 60×60 system. And also as before, there are significant fluctuations associated with the horizontal strip ordered phase. Interestingly, in the 60×60 system $\Delta(0,1)$ actually has a broad secondary peak in the ordered phase. This was quite unexpected and awaits a satisfactory explanation. For now, we only note that lowering T increases the effective bias, E/T , and therefore enhances fluctuations associated with the drive. Lowering T further we observe $S(0,1)$ falling abruptly, while $S(1,0)$ climbs rapidly, suggesting a discontinuous transition from the horizontal strip into the vertical strip. In the neighborhood of such a tran-

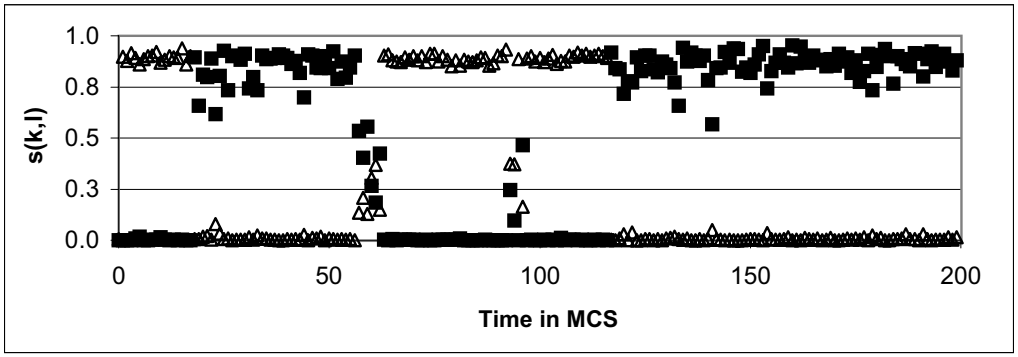

Figure 2.8: Timetrace at $T = .832$. Time in units of $.2M$ MCS is plotted on the horizontal axis. The values of $s\,(0,1)$ and $s\,(1,0)$ (triangles and squares, respectively) are plotted on the vertical axis.

sition, one expects to see metastability of the unfavored phase, and this is indeed the case as shown in figure 2.8. Here we have plotted *time traces* (as opposed to configurational averages) of structure factors for individual configurations, $s\,(1,0)$ and $s\,(0,1)$, defined in eqns. (2.4). When $s\,(1,0)$ ($s\,(0,1)$) $= 1$ the configuration is a perfect vertical (horizontal) strip. Sufficiently close to the transition, the time traces reveal the expected behavior, as the system switches between the two ordered phases. Notice the length of the run shown: $40M$ MCS, which is a factor of 40 longer than typical runs, indicating that the lifetimes of metastable configurations are already quite long even in the 40×40 system. Such behavior is therefore nearly unobservable in the 60×60 system.

At smaller values of f we are nearing the junction of the three phase boundaries, which considerably complicates the analysis of data from small systems in two ways. The sequence of transitions (DO-TS followed by TS-PS) becomes difficult to resolve, as they are quite close in temperature, and massive fluctuations from the first-order TS-PS line may wash out the signal in $\Delta(0,1)$ which locates the continuous DO-TS line. And if the junction of the three lines is indeed a nonequilibrium bicritical point, we can expect unexplored finite-size effects to interfere with the analysis. We can, however, make some progress based on the assumption that the relevant control parameter near the bicritical point is the number of rows of the minority

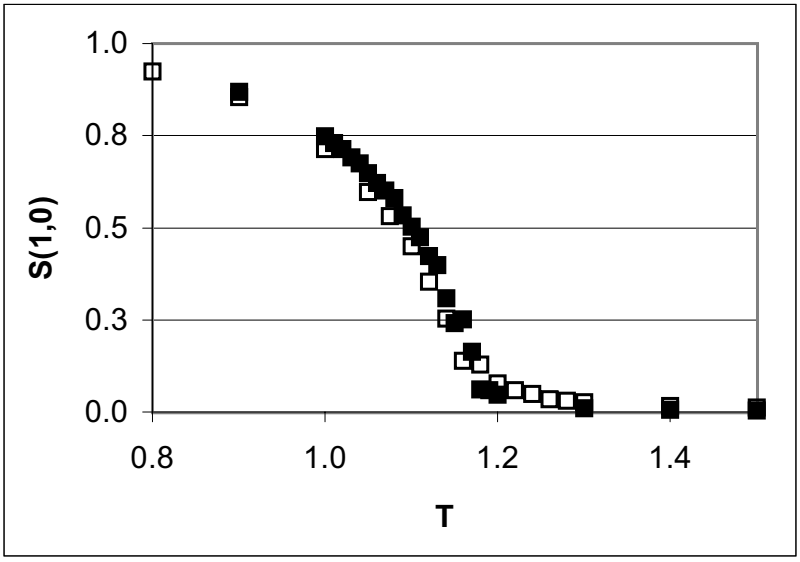

Figure 2.9: $S\,(1,0)$ as a function of T for $f = .025$. 40×40 (60×60) data are shown by open (filled) squares.

species. This hypothesis will be treated in more detail below, in the sections on scaling arguments.

At precisely one row of the minority species it is no longer possible to accurately resolve the two transitions in the 40×40 system. A weak transverse ordering is observed, with $S(0,1)$ reaching at most 40% of perfect order. At this f, the minority species forms a 'cloud', which localizes the majority species without forming a distinct interface. In the vicinity of the PS-TS first-order transition, huge fluctuations associated with switching between metastable configurations are observed, which wash out the signal of the DO-PS transition. However, it is interesting that these transitions can be observed in larger systems at precisely one row of the minority species. In the larger systems these two transitions are sufficiently far apart in temperature that they can be resolved; we will see below that T_c increases with L_y across the DO-TS transition. This likely explains why the DO-TS transition is not observed in the 40×40 system.

Below one row of the minority species we no longer observe the transverse order, though we caution that this may be strictly correct only for the *finite* system. At just below a single row of the minority species, the high temperature phase is homogenous and the low temperature phase is the parallel strip.

In the vicinity of the transition, huge fluctuations are observed in $S(0,1)$ and especially $S(1,0)$, where the fluctuations are an order of magnitude larger than the signal at the DO-TS boundary. In this region neither $S(1,0)$ nor $S(0,1)$ posesses a well-defined average; timetraces indicate vigorous competition between the two ordered phases. We conjecture that we are here close to the bicritical point in the finite system, and are therefore unable to resolve the transition without some knowledge of the scaling to guide the analysis.

At still smaller f we are farther from the bicritical point, and the complications from the presence of the minority species are less severe. Figure 2.9 shows $S(1,0)$ for two system sizes at exactly one-half row of the minority species. We have not shown $S(0,1)$, as the signal has become insignificant. $S(1,0)$ shows the low temperature configuration to be a single parallel strip, the smooth approach to zero again suggesting a continuous transition. And indeed, the data for $\Delta(1,0)$ is consistent with this conjecture, with a sharp peak which increases with system size. The amplitude of the peak is smaller by a factor of five than the peaks observed near the bicritical point, where we found the fluctuations were not associated with a well-defined average, but rather were associated with transitions into and out of the ordered phase. Here the amplitude of the peak suggests that it is associated with fluctuations about a well-defined average. Timetraces in the vicinity of the transition support this conjecture.

Charge currents were also measured in order to look for signatures of the various phases and transitions. We note however that as we are changing T, we are also changing the *effective* bias $\varepsilon = E/T$, and therefore a more appropriate quantity is the conductivity, $\kappa \equiv j/\varepsilon$. In figure 2.10 we plot κ as a function of ε for each f discussed in this and the following sections; we present only data for the 40×40 system as there are no significant differences between the two system sizes. At temperatures below $T = 1.4$ ($\varepsilon > 1.4$) the conductivity vanishes in the $f = .50$ systems; as the temperature is raised the effective drive is reduced, and backward hops occasionally occur, allowing a small current to trickle through the blockage. Upon raising the temperature further, the conductivity changes slope at $T = 3.6$ ($\varepsilon = .56$) in the 40×40 system, which *does not* coincide with the phase transition. Rather the maximal conductivity occurs in the disordered phase, but at a temperature which is not too large, so that backward hops are not so common as to begin reducing the current. The transition apparently corresponds instead to the *inflection point* ($T = 3.4$, $\varepsilon = .59$), where the curvature changes sign. At $f = .10$, the conductivity has a slope discontinuity in the

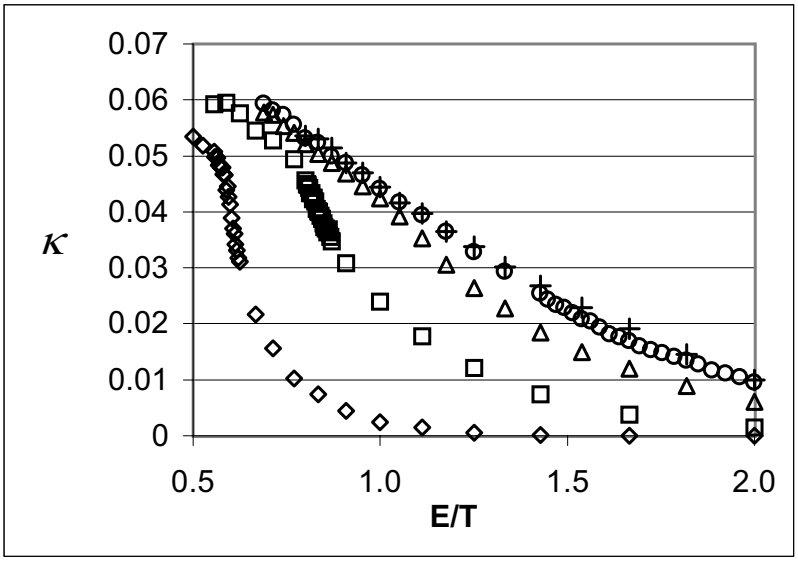

Figure 2.10: Conductivity as a function of effective drive E/T for several f's. $f = .50$, diamonds; $f = .10$, squares; $f = .075$, triangles; $f = .05$, circles; $f = .04$, +'s.

40×40 system at $T = 2.6$ ($\varepsilon = .77$), slightly above the critical temperature $T_c = 2.4$ ($\varepsilon = .83$). Though there must be an inflection point in κ near the transition, our data are not precise enough to locate it. At $f = .075$ and below, the conductivity drops smoothly to zero with T, showing no indication of either transition. Apparently S and Δ are far more sensitive to the transitions in our model.

Scaling Arguments

Now that we have surveyed the phase diagram in some detail, we turn to look closely at some of the boundaries with the help of some scaling arguments. Looking again at figure 2.1, we note two potentially troubling features. First, there is a shift in T_c across the DO-TS boundary of about 50% between the two system sizes. We will treat this using a mean-field scaling argument. Second, we note that the bicritical point has shifted towards the $f = 0$ axis in the larger system. It has been alluded to in previous paragraphs that some insight is had by considering the number of rows of the minority species, rather than the fraction f. We will look more closely at this suggestion by considering some larger systems and rectangular geometries. Finally, we look at the $f = 0$ phase transition, using scaling arguments developed for the KLS

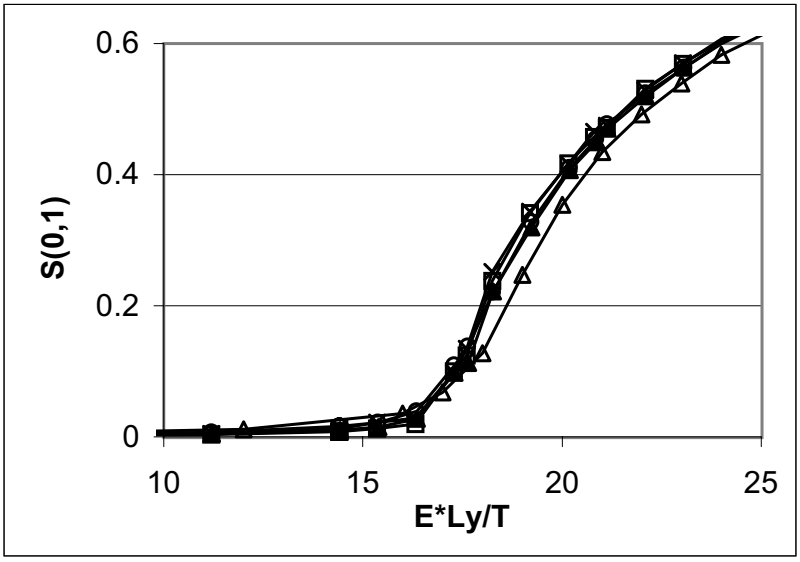

Figure 2.11: $S(0,1)$ as a function of effective drive for $J = 1$. System sizes: 40×40, open triangles; 40×60, circles; 40×80, $\times$'s; 60×60, filled triangles; 60×80, squares.

model.

The shift in T_c with system size is most pronounced at $f = .50$. Previous work on the two-species model with $J = 0$ treated the ordered phase in a mean field approximation by solving equations of motion for the two different charge densities[27]. It was found that the scaling functions depend on the combination EL_y/T , indicating that the effective bias E/T introduces a new length scale. This scaling implies an infinite-volume limit in which $E/T \to 0$ as $L_y \to \infty$, while keeping the combination fixed. Analysis of the *ordered phase* based on these ideas has worked quite well, so that we now attempt to extend this approach to analyze quantities near criticality and for $J \neq 0$. There is no reason to expect success *a priori*, as both critical fluctuations and nonzero J may modify the mean-field exponents. In figures 2.11 and 2.12 we have plotted $S(0,1)$ and $\Delta(0,1)$ for $J = 1$. (We have rescaled $\Delta(0,1)$ by the volume in order to compare different system sizes.) Rather than crossing the phase boundary by varying T we have opted instead to vary E; in this way we can change the effective bias E/T without changing the interaction strength, J/T. While the collapse of $S(0,1)$ in fig. 2.11 is not perfect, the mean-field scaling argument accounts for most of the shift in T_c. There is a shift in the

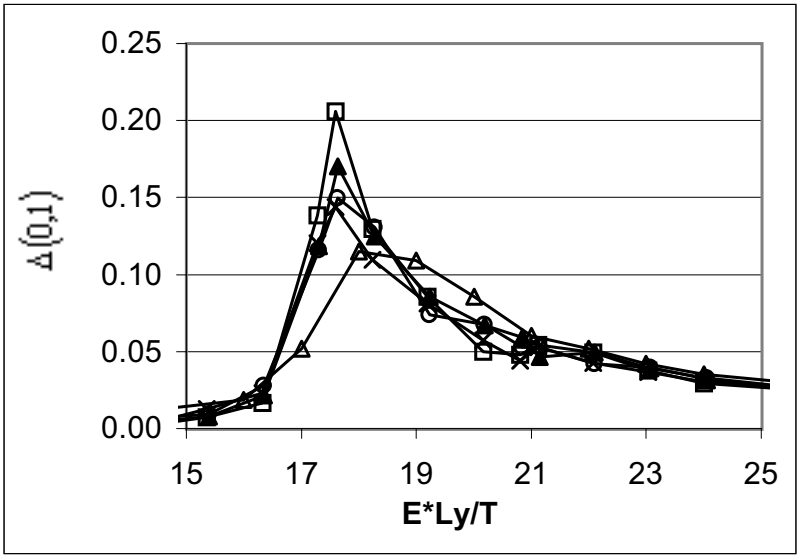

Figure 2.12: $\Delta(0,1)$ as a function of effective drive for $J = 1$. Symbols same as previous figure.

peak of $\Delta(0,1)$ of about 3.6% between the largest and smallest systems, if the same data were plotted without rescaling the shift in T_c is about 52%. Also of note is the extremely weak dependence on the transverse dimension, as predicted by the scaling argument. We also examined the same quantities for $J = 0$. Interestingly, the data collapse for $J = 1$ is better than in the $J = 0$ case. This is somewhat puzzling, as the original scaling argument was derived for $J = 0$, and we would expect the interactions to perhaps modify the scaling behavior. Whatever the resolution of this mystery, it is apparent that the scaling argument presented here accounts for the pronounced shift in T_c seen in the phase diagram; increasing L_y requires a corresponding decrease in the effective bias E/T, which at fixed E implies an increase in T.

Another issue concerns the location of the junction of the three phase boundaries, shown in figure 2.1. It is clear that the junction moves toward the $f = 0$ axis as the system size is increased. In fact, in both systems the boundaries merge just below a *single row* of the minority species, which naturally corresponds to a smaller f in the larger system. In figure 2.13 we have replotted the data from figure 2.1, replacing f with $fL_y/2$, which is simply the *number of rows* of the minority species. Near the junction of the three lines we have also included results from a few other system

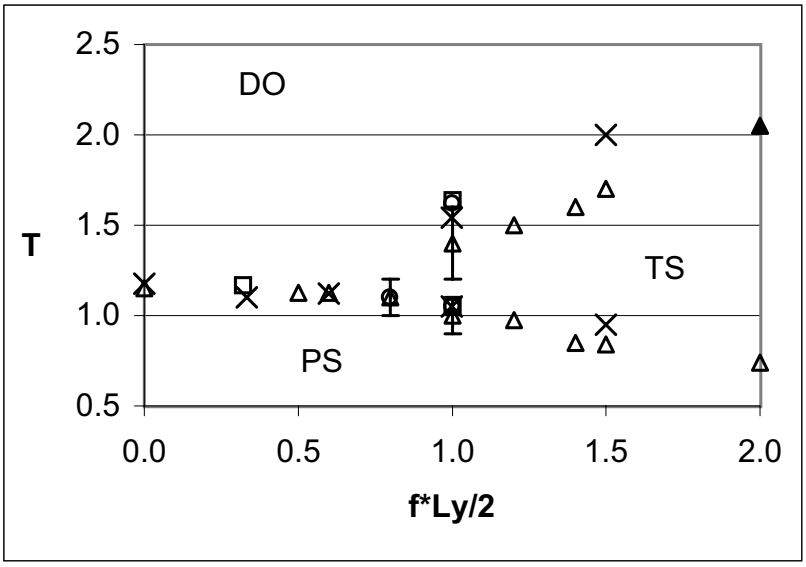

Figure 2.13: $f - T$ plane, f rescaled to represent the number of rows of the minority species. System sizes: triangles, 40×40; circles, 40×80; $\times$'s, 60×60; squares, 60×80.

sizes with rectangular geometries. In these variables the junctions of the boundaries coincide, within the error bars, for all system sizes, suggesting that the onset of the two-species order occurs, at least in relatively small finite systems, when there are sufficient minority particles to form a single row. The crucial question concerns the extrapolation of this result to an appropriate thermodynamic limit. If the system size goes to infinity in the most naive way, i.e., $L_x, L_y \to \infty$ at fixed aspect ratio L_x/L_y, the particle density associated with a 'single row' vanishes. It is possible that the DO-PS transition exists in an infinite volume only at $f = 0$, and any *finite density* of 'disorder' (i.e., the minority species) induces the two-species order. Work in progress considers the KLS model in the presence of such disorder in order to discover how it modifies the phase diagram. We will have to leave discussion of this issue to a future publication, and for now limit ourselves to statements about the finite systems.

At $f = 0$ there is only one species, and we observe the KLS transition at *finite* E. Though a great deal of study has been devoted to this transition at infinite E, there has been no detailed work at finite E. Here we present a finite-size scaling analysis of this transition, in order to locate $T_c\,(E = 2.0)$,

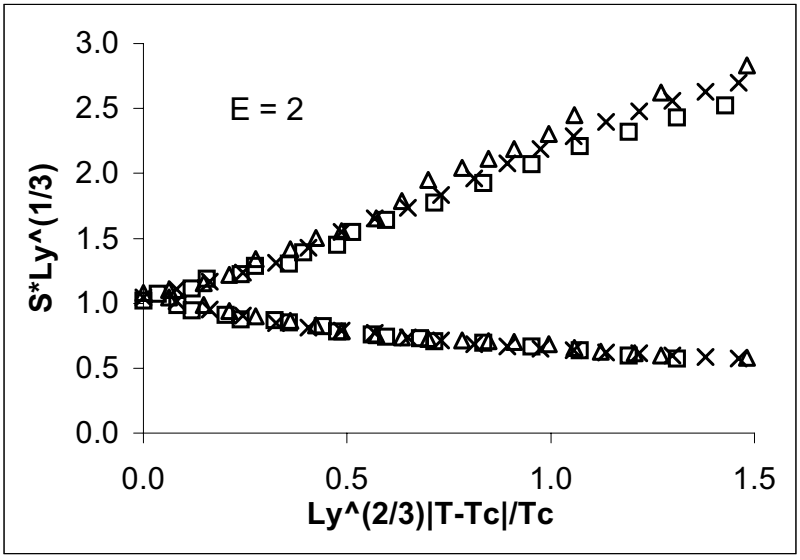

Figure 2.14: Anisotropic scaling plot of $S(1,0)$ at $f = 0$, $E = 2.0$.System sizes: Squares, 24×54; $\times$'s, 28×86; triangles, 32×128.

and also to demonstrate the subtleties which can arise when studying phase transitions with anisotropic, nonequilibrium dynamics.

Field theoretic studies of the KLS model[24] indicate that the critical behavior is strongly anisotropic, meaning that correlation lengths diverge with different exponents in the field direction and perpendicular to the field. Specifically, the fluctuations perpendicular to the field are gaussian $\left(\nu_\perp = \frac{1}{2}\right)$ while those parallel to the field are not $\left(\nu_\parallel = \frac{3}{2}\right)$. Correlation lengths therefore grow faster in the parallel direction, suggesting an analysis of rectangular samples such that the anisotropic aspect ratio $A \equiv L_\parallel^{\nu_\perp/\nu_\parallel} L_\perp^{-1}$ is held fixed[22]. While there was some discussion regarding the correct mesoscopic model[25], detailed numerical simulations have shown that the exponents cited above are the correct ones[21],[23]. In the following we will use only the phenomenological result of Leung for the scaling of the order parameter at fixed A:

$$S\left(T, L_\parallel, L_\perp\right) = L_\parallel^{-\beta/\nu_\parallel} \overline{S}\left(t L_\parallel^{1/\nu_\parallel}, A\right) \tag{2.5}$$

where S refers to $S(1,0)$. A detailed discussion of the subtleties of the FSS analysis for the KLS model and precision numerical results can be found in[21].

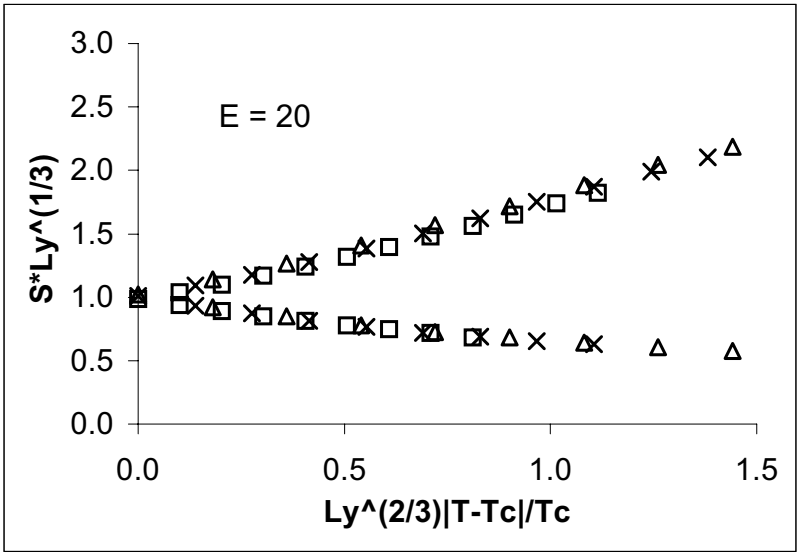

Figure 2.15: Anisotropic scaling plot of $S(1,0)$ at $f = 0$, $E = 20.0$. Symbols same as in fig. 2.14.

Figure 2.14 presents our data for the scaled order parameter at $E = 2$; the same data for saturation E is shown in fig. 2.15[34]. This data is not intended as a test of the mesoscopic model, it merely is meant to indicate that the exponents at infinite E are consistent with those at finite E, and to determine $T_c(E = 2.0) = 1.20(2)$. The data collapse is comparable to that seen at saturation E, with the high temperature (lower) branch collapsing quite well and the low temperature (upper) branch showing systematic deviations from scaling. Similar behavior is observed in the scaling of the order parameter fluctuations, though the data are a bit noisier, owing to the fact that the fluctuations are a function of higher moments of $n(\mathbf{r})$. These deviations remain unexplained. Possibly they are due to corrections to scaling or perhaps the asymptotic region is only observed very close to T_c.

In the above analysis, we determined T_c based solely on the quality of the data collapse. Such an estimate of course relies on assuming a particular set of exponents, which are used when rescaling the data. This circular dependence fuels arguments regarding the correct value of T_c and critical exponents. It is therefore desirable to estimate T_c independent of assumptions about exponents. For a system described by the Landau-Ginzburg-Wilson (LGW) Hamiltonian, this can be accomplished by considering the asymp-

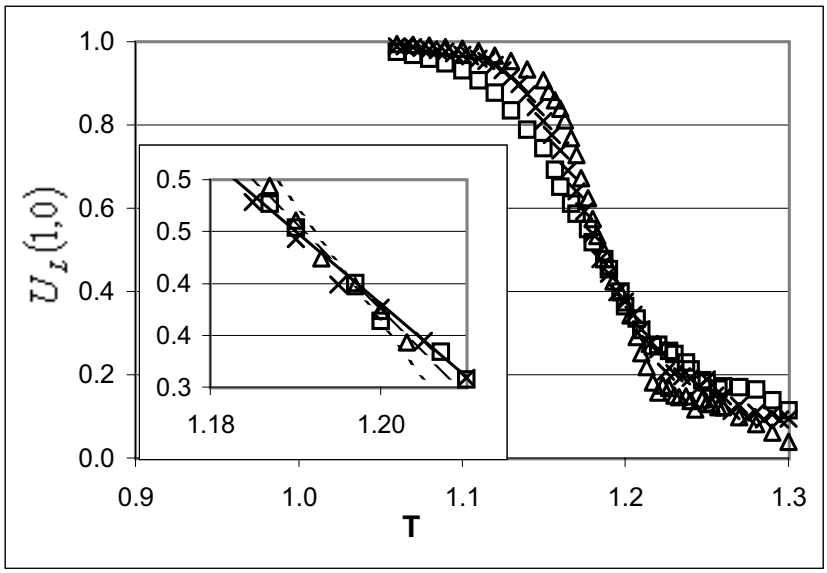

Figure 2.16: $U_L(1,0)$ at $f = 0$, $E = 2.0$.Symbols same as in fig. 2.14.Detail of the intersection is shown in the inset.

totic behavior of the 4^{th} order (Binder) cumulant, U_L, which in our language is defined by: $U_L \equiv 1 - \langle S^4 \rangle_L / 3 \langle S^2 \rangle_L^2$[35]; the subscript L is a reminder that this quantity depends on the system size. U_L is essentially the coupling u associated with the ϕ^4 nonlinearity in the LGW Hamiltonian. In dimensions $d < d_c$, u will take its universal value at T_c. Sweeping in T and plotting U_L for different system sizes will yield a plot similar to fig. 2.16, where we have plotted U_L for the *driven* case, with $E = 2.0$. Of course, the driven case is not described by the LGW hamiltonian, but by an anisotropic generalization with an additional nonlinearity that is proportional to the drive[24]. In fact, the field theory for the driven system predicts that u is only dangerously irrelevant, while the $\mathcal{E}$ nonlinearity is the most relevant. In this model, therefore, there is no fixed point associated with u, and the data in fig. 2.16 should not cross each other at a unique point. So why do we observe an incredibly precise intersection? One possibility is that we are observing effective Ising critical behavior. At $E = 2.0$, the energy gained from a favorably biased hop is only one-half the energy gained by forming a nearest-neighbor bond. Indeed, no crossing is observed in the $E = 20.0$ system. Though this last observation suggests that we are indeed observing the proximity of the Ising fixed point in the $E = 2.0$ data, certainly more work is needed to further

clarify the issue. For example, a flow diagram for U_L as a function of system size ought to clearly differentiate between a nontrivial fixed point and gaussian fluctuations[35].

We close this section on the $f - T$ phase diagram with some comments on unaswered questions. The picture in the high f limit is clear: a clean continuous transition into the horizontal strip, with T_c decreasing with f. When f is reduced until there are approximately three rows of the minority species there remains a clear signal of the transition, though it now sits atop a shoulder of fluctuations of the ordered phase. At yet smaller f there also appears a second transition between the two ordered phases at lower T; it has characteristics of a first-order transition. At even lower f, at approximately one row of the minority species, both fluctuations perpendicular and parallel to E become so violent that the DO-TS transition is only seen in larger volumes, as the two transitions nearly overlap in the 40×40 system. Close to the $f = 0$ point, the transition is once again clean and apparently continuous into a vertical strip of mixed charge. Of course, all the statements in this paper are for finite systems. In order to draw robust conclusions, a more systematic analysis of larger samples is required. We have seen how complex and subtle are the issues surrounding the transition at $f = 0$. Perhaps a fruitful way to proceed when $f \neq 0$ is to adopt the technique introduced by Caracciolo *et al*[21], directly measuring finite volume correlation lengths for various geometries and volumes. In this way we may develop some understanding of how to approach the infinite volume limit in a simple way, minimizing corrections to scaling which would complicate an uninformed analysis.

2.2.2 Phase diagram in f and E

In the preceding section we studied a slice of the phase diagram at constant E, varying the fraction of the minority species and the temperature. Varying T effectively varies both the strength of particle-particle attractions *and* the strength of the bias, recall that the quantities which enter the rates are J/T and E/T. In this section we would like to study a different slice of the phase diagram. By varying E and f at fixed T, the interparticle attractions are held constant while the strength of the bias is varied. In this way we can study directly the competition between the drive and the attractive interactions. The program is the same as before, except now a value is chosen for T, and we then scan in E for several values of f. The values of T are chosen by reference to the KLS temperature: $T = 2.0$ is above the critical temperature

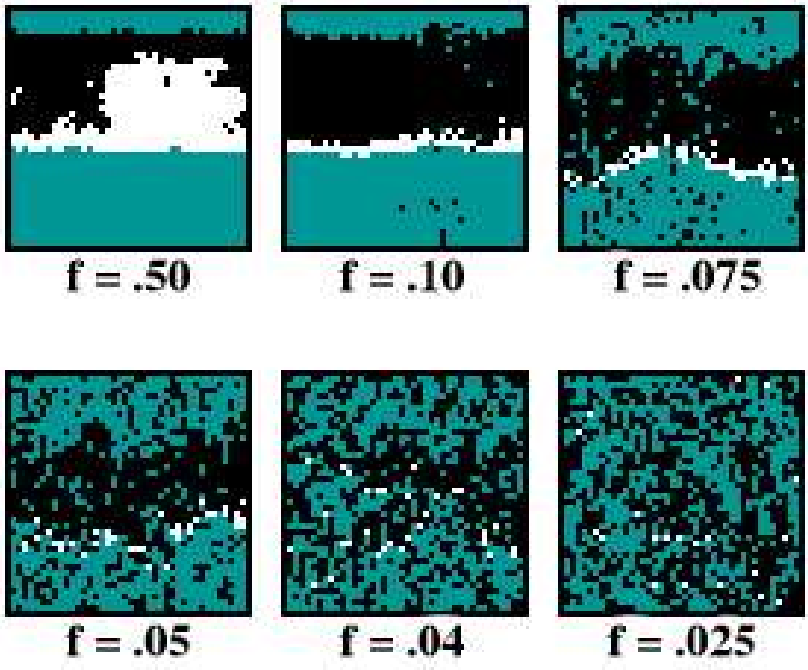

Figure 2.17: Configurations for several f's at $E = 20$, $T = 2.0$.

of the KLS model at saturation, and $T = 1.2$ is at the critical temperature for $E = 2.0$, studied in the previous section. At this stage, we have only data for 40×40 systems, and therefore we are unable yet to even speculate on results for larger volumes. We present this data first as a preliminary investigation, and second as an extension of the detailed results in the previous sections. By looking at a different slice of the phase diagram we will be able to see the above results in a new light.

T = 2.0

As in previous sections, we first survey the phase diagram with the help of some typical configurations. The qualitative picture will then be made more quantitative in the next section, by examining the behavior of currents and order parameters.

Figure 2.17 shows a series of configurations at various f for $E = 20.0$. The first frame clearly shows the transverse strip at $f = .50$, and the absence of travelers suggests that the strip is stationary. In the next frame we have reduced f to .10, reducing the thickness of the minority species to exactly two rows. Consequently we now see some travelers trickling through a break in the blockage. Watching an animation in this region of the phase diagram

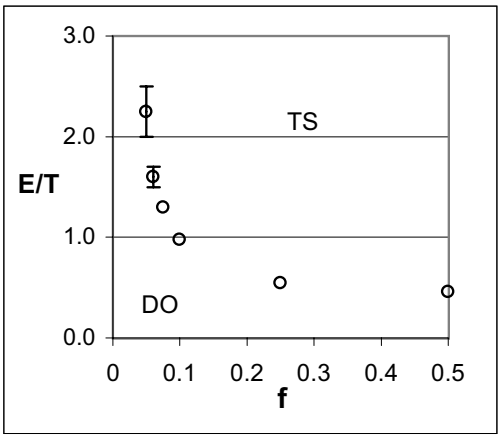

Figure 2.18: Phase diagram in f and E/T at $T = 2.0$. Disorder(DO) is observed at small f and E, transverse strip(TS) at high f and E.

reveals an interesting behavior: the strip is mostly quiescent, except for a few particles hopping back and forth at the particle-hole interface. Aside from the different ratio of + to −, these configurations look similar to the $f = .50$ strip. Then, a sudden large fluctuation opens up a hole in the minority blockage: the + particles pour through, and the strip fluctuates and drifts partway around the lattice, until the blockage is reestablished. Reducing f further to .075 (third frame) we see a strip in the middle of one of the

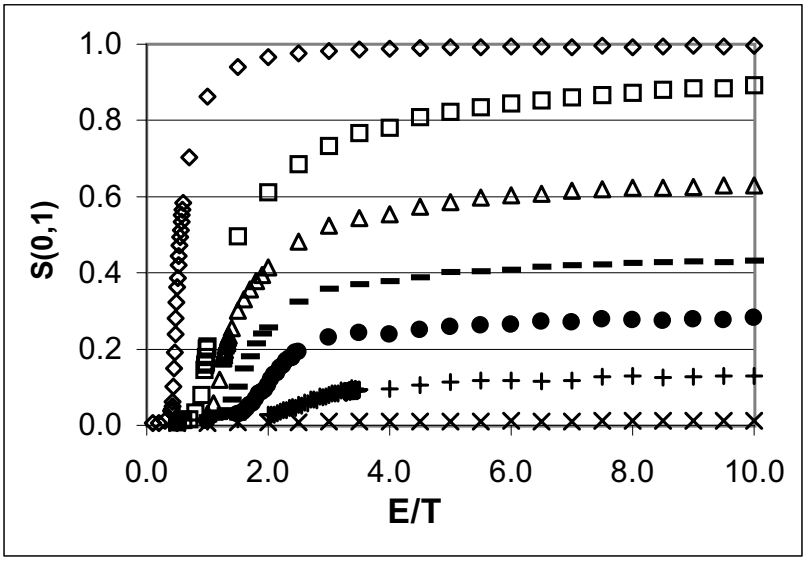

Figure 2.19: $S(0,1)$ as a function of E/T for several f's. $f = .50$, diamonds; $f = .10$, squares; $f = .075$, triangles; $f = .06$, −'s; $f = .05$, circles; $f = .04$, +'s; $f = .025$, ×'s.

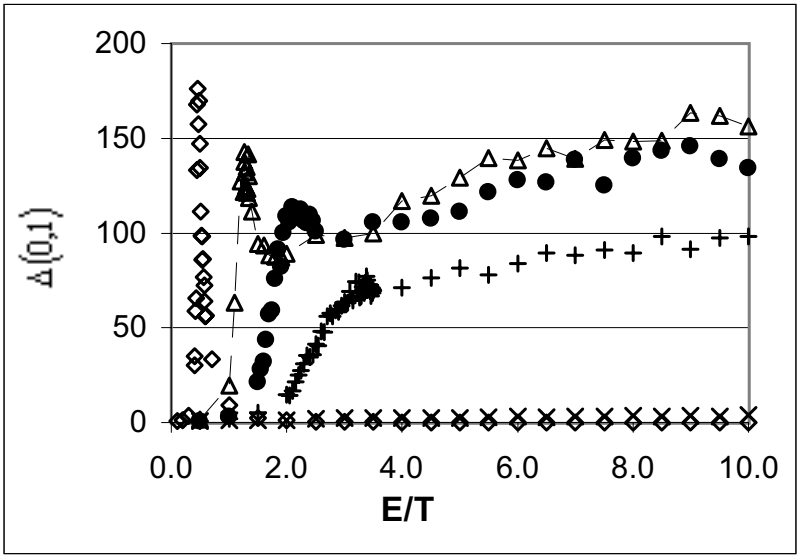

Figure 2.20: $\Delta(0,1)$ as a function of E/T for several f's. Symbols same as previous figure. A line has been added to $f = .075$ to make the figure clearer.

fluctuation events just described. In the fourth frame, we set $f = .05$, and while the strip is still clearly visible it now drifts continuously and is unable to sustain the long-wavelength fluctuations just described. Here we see an example of the 'localizing cloud' of minority particles which was mentioned in sec. 2.2.1. The final two frames show $f = .04$ and .025. Now there is no longer any clear evidence of phase separation. This rough picture is consistent with our earlier investigation of the two-species transition, where we found that two-species order is observed at and above a single row of the minority species.

Figure 2.18 presents the phase diagram at $T = 2.0$. The boundary separates a horizontal strip at high E and f from a homogenous phase at small E and f. As we are above the critical temperature for the KLS model at saturation bias, the vertical strip does not appear at any E; at low f (where we might otherwise expect to see such ordered configurations) the system simply remains disordered for any E and f. Figures 2.19 and 2.20 show $S(0,1)$ and $\Delta(0,1)$ for several values of f; in the interest of clarity $\Delta(0,1)$ is plotted for only four f 's. As E is increased the system orders into a transverse strip, with $S(0,1)$ saturating at smaller values as f is decreased. At $f = .05$ (exactly one row of the minority species) S saturates at only .28, indicating

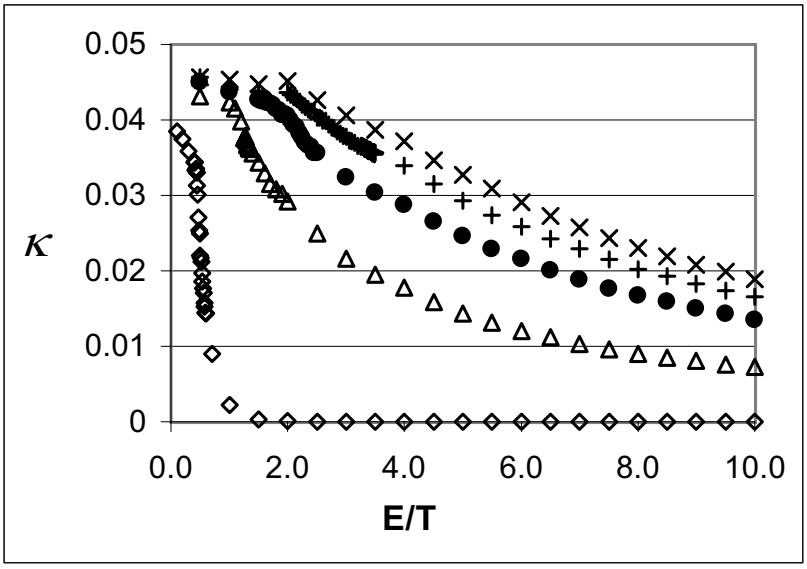

Figure 2.21: Conductivity as a function of effective drive. Symbols same as in Fig. 2.10

that the transverse ordering is rather weak, though comparison with the data for $f = .025$ shows dramatically different behavior. Here $S(0,1)$ reaches a maximum of only .01, and the behavior can hardly be called 'saturation'. $\Delta(0,1)$ also signals a transition, though the clean, sharp spike at $f = .50$ becomes a broad bump at $f = .05$, and shows no signal at $f = .025$. Remember that f is fixed, and we scan in E. Since the phase boundary in fig. 2.18 is nearly vertical at small f, we are crossing the boundary at a shallow angle, which may account for the weaking of the signal in $\Delta(0,1)$. The susceptibility also indicates a difference in the ordered phases at different f: at large f increasing E supresses fluctuations, while at smaller f (when the strip begins drifting) increasing E enhances fluctuations. It is important to note that the fluctuations at high E are fluctuations about the ordered phase, as $\Delta(0,1)$ is always $2-3$ orders of magnitude larger than $\Delta(1,0)$. Though the data is not included in the plots, we have checked the behavior of the ordered phase for values of E as high as 40. The fluctuations for small f ($f < .10$) saturate and bounce around a well-defined average, while for larger f they are suppressed. This is true for $f = .05$ and greater; at $f = .025$ the magnitude of fluctuations in either direction are comparable.

Finally, we consider the conductivity across the phase boundary, plotted

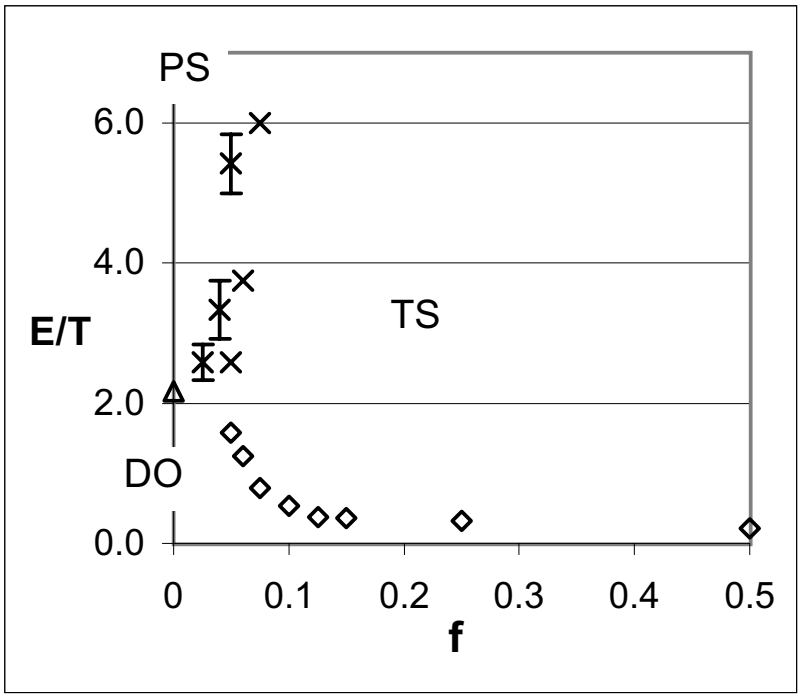

Figure 2.22: Phase diagram in E/T and f for $T = 1.2$. A continuous boundary separates DO from TS (diamonds) as well as DO from PS (triangles). $\times$'s indicate a possible boundary between TS and PS.

for several values of f in figure 2.21. As before, the transition apparently corresponds to the inflection point of the conductivity, though in these data this point is visible at $f \geq .05$. Indeed, there is a qualitative difference between $f > .05$ and $f < .05$; the conductivity at smaller f lacks an obvious inflection point. Though these data are not particularly revealing, it will be interesting to compare them to the conductivity data at $T = 1.2$.

T = 1.2

In the preceding section we found a simple phase diagram, with a single boundary separating two-species order from the homogenous phase. Since the temperature was chosen well above the maximum KLS transition temperature, $T_{KLS}\,(E = \infty) = 1.414$, the KLS ordered phase could not be observed. Now, we lower the temperature to $T = 1.2 < T_{KLS}$ and explore the corresponding (f-E) slice of the phase diagram (Fig. 2.22). As long as we remain at $f > .10$, we observe a transition similar to the one at $T = 2.0$: from the homogenous phase into two-species order. In contrast, for $f < .04$ the KLS transition is observed, since the minority species is too scarce to form

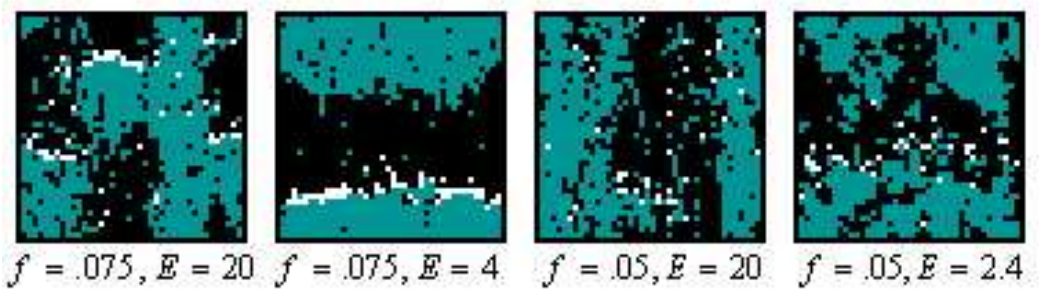

Figure 2.23: Typical configurations for the $T = 1.2$ plane.

a blockage and $T < T_{KLS}\,(E = \infty)$. Between these two limiting values of f we are again in the vicinity of the bicritical point, and the situation becomes complicated by the competing types of order.

Figure 2.23 shows typical configurations at 2 f's for various E. For $f >$ .075 these configurations look much as they did at $T = 2.0$, so they have been omitted. The $f = .075$, $E = 20.0$ configuration shows some very interesting structure, almost 'equal parts' KLS and two-species order, suggesting some serious competition between the two phases. We stress that this is a *typical* configuration. When f is reduced to a single row ($f = .05$) this competition is reduced, and we see instead a KLS phase with some local two-species order. This trend continues upon reducing f to zero, where at high E the KLS order is observed. The other panels show $f = .075$ and .05 at smaller values of E, $E = 4.0$ and 2.4 respectively. These E values were chosen because they maximize the two-species order for these f's. In each case the strip drifts rapidly around the lattice. Interestingly, as the majority species is piled onto the back of the drifting strip it builds long fingers, leading to a very irregular interface. Pictures at smaller f's are not shown, as they do not form the transverse strip at smaller E. In the next section we locate these boundaries and study the phases in greater detail by examing the behavior of S, Δ, and κ.

In fig. 2.24 we plot S for the high f phases. For $f = .50$ and .10, $S\,(0,1)$ shows the system ordering into the two-species phase much as in the previous section. There is, however, one notable new feature for $f = .10$, where we see a slight suppression of $S\,(0,1)$ over an intermediate range of E, from about $E = 6.0$ to $E = 20.0$. In this range backward hops occur often enough

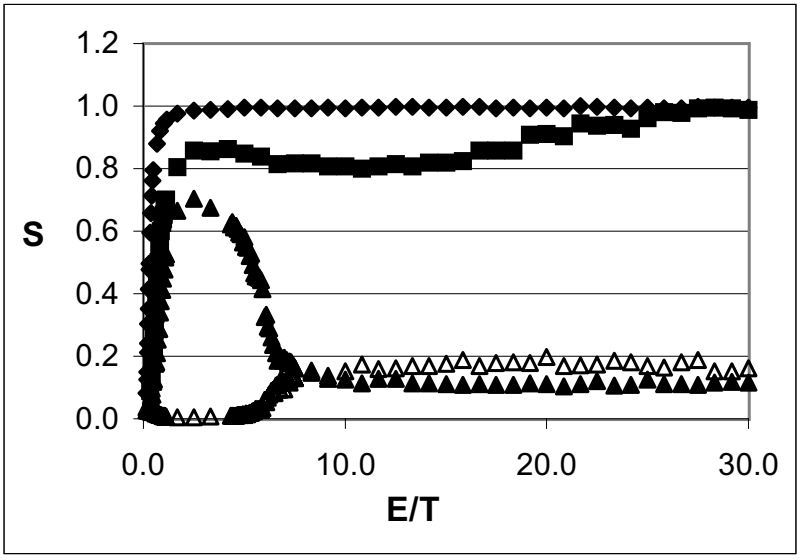

Figure 2.24: $S(0,1)$ as a function of E/T for several f's. $f = .50$, diamonds; $f = .10$, squares; $f = .075$, filled triangles. Open triangles indicate $S(1,0)$ for $f = .075$.

to occasionally open a hole in the minority blockage, allowing the majority species to pour through until the blockage reforms. Increasing E reduces the likelihood of such events, until the strip is perfect except for some surface diffusion at the particle-hole interface. At $f = .075$ the behavior changes dramatically. After maximizing the two-species order at $E = 4.0$, increasing E further supresses $S(0,1)$ and enhances $S(1,0)$, until both level off below .2. The system can hardly be said to have switched to KLS order, though neither is it precisely disordered either. Recall that T (and therefore J/T) is held constant, so that increasing E stabilizes interfaces parallel to E, as in the KLS model. The number of the minority species is however large enough to destabilize the parallel strip by forming within it bubbles of local two-species order. Apparently the competition between the two phases is very balanced in this small system. It would be interesting to look at some larger systems and see whether this 'competitive' phase is maintained, or whether the KLS order becomes stable.

We can learn more about these transitions by considering the susceptibilities. Observations of $\Delta(0,1)$ are consistent with a continuous transition from disorder into the transverse strip at small E. *The behavior is like that seen*

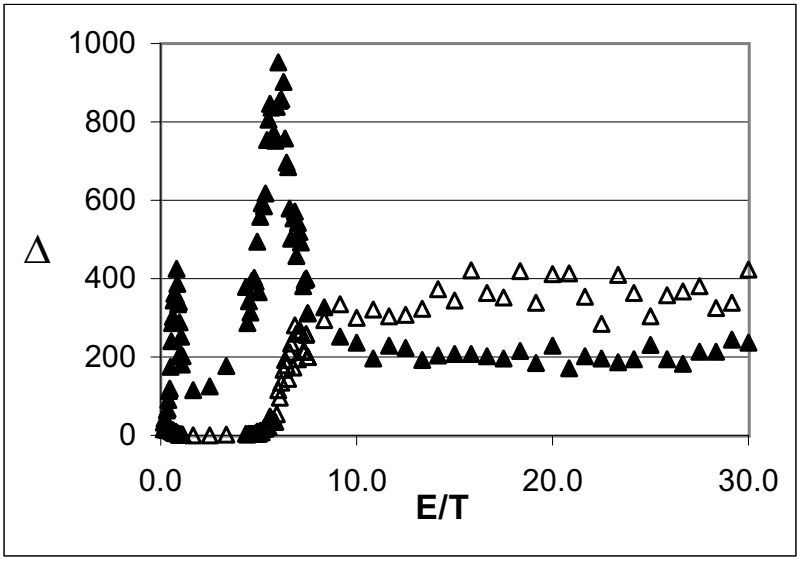

Figure 2.25: $\Delta(0,1)$ (filled triangles) and $\Delta(1,0)$ (open triangles) as a function of E/T for $f = .075$.

near the same boundary in the previous sections; here we are observing the same transition at *fixed* J and T. In fig. 2.25 we show $\Delta(1,0)$ and $\Delta(0,1)$ for $f = .075$. Here we observe a second peak in $\Delta(0,1)$ at $E = 7.2$, which corresponds to a value of about $S = .4$ in fig. 2.24. This peak is rather broad and more than twice the amplitude of the one associated with the DO-TS transition. Perhaps it suggests a first-order transition which would be observed in a larger system, separating the two-species phase from the KLS phase. Then at higher E both $\Delta(0,1)$ and $\Delta(1,0)$ bounce around nonzero values, indicating the fluctuations of the competitive phase. We note no signal of a transition in $\Delta(1,0)$.

We now continue by looking at the data for $f = .05$, shown in fig. 2.26, where we have plotted S for each type of order. We observe that the transverse strip only makes a brief appearance, with $S(0,1)$ reaching a maximum of only .35. Then at higher E the parallel strip wins and fluctuates around a value of about .41. We note that the high E phase here is not the competitive phase seen just previously at $f = .075$, as there is no signal in either $S(0,1)$ or $\Delta(0,1)$. However, there is not either any real signal of a tranisition between the two types of order. There is a vague remnant in $\Delta(0,1)$ of the double peak structure seen at $f = .075$, and then a broad, indistinct signal

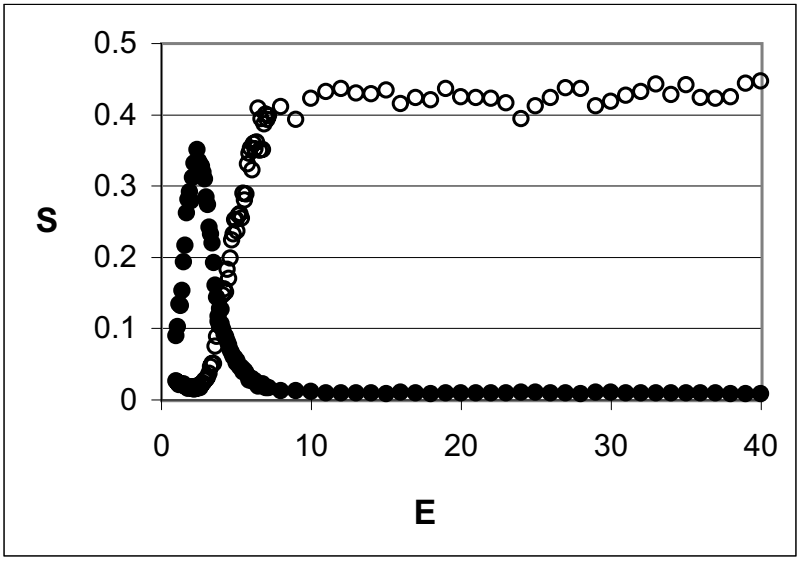

Figure 2.26: $S(0,1)$ (filled circles) and $S(1,0)$ (open circles) as a function of E/T for $f = .05$.

in $\Delta(1,0)$ before it settles down to describe the fluctuations of the ordered phase. Only further investigation of larger systems can determine whether these weak signals in fact signal a transition. Upon reducing f below .05 we find that the transverse strip has essentially disappeared. Meanwhile, $S(1,0)$ looks as it does in fig. 2.26, saturating to about .50, indicating that the KLS strip has formed. Apparently the system is unable to completely order at any E, as $T_{KLS}(E = \infty) = 1.4$. We stress that this behavior is due to the proximity of the KLS phase transition, not due to some residual competition with the transverse strip. Finally, we note that the behavior of the susceptibility is consistent with a continuous transition into the parallel strip.

The conductivities are shown in fig. 2.27. At $f = .50$ and .10, κ has much the same form as seen before, decreasing monotonically with E. This is no longer the case when f is reduced to .075. Now κ develops a broad minimum which coincides with the appearance of the two-species order, followed by a small peak at $E = 8.0$ before falling off with E. The peak coincides with the crossing of $S(0,1)$ and $S(1,0)$, which suggests that the current is maximized by the competitive phase. With the current maximized, increasing E simply reduces κ; indeed the raw data for the current shows that this is the case.

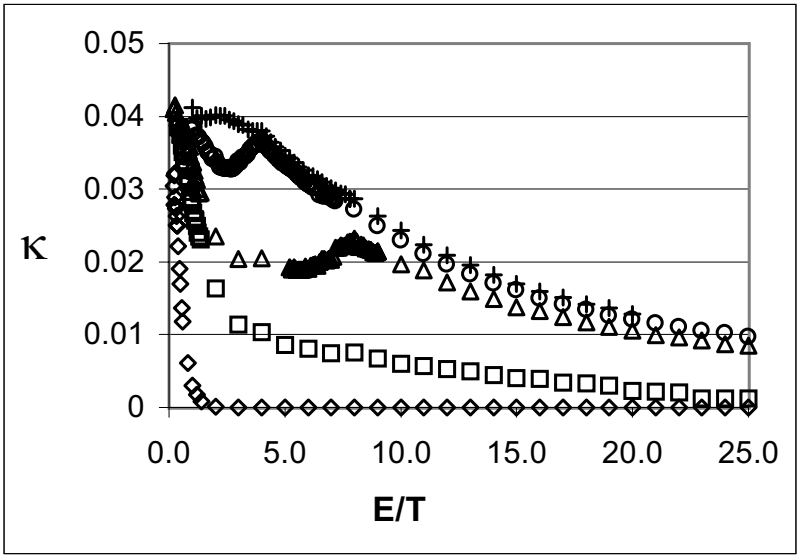

Figure 2.27: Conductivity in the $T = 1.2$ plane as a function of E/T for several f's. Symbols same as Fig. 2.10.

The data for $f = .05$ shows the same nonmonotonic structure as for the $f = .075$ data. Again, the peak corresponds to the crossing of the two order parameters, and then falls off with increasing E. This similarity suggests that perhaps the high E phase at $f = .075$ is in fact the parallel strip, and such behavior would be observed in a larger system. For values of $f < .05$ we no longer observe the secondary peak, nor do we observe the competitive phase. We must, however, leave questions about the nature of the high-E phase open to further study.

2.3 Summary

We have just presented a sketch of the phase diagram at two different fixed T's, by varying f and E. At $T = 2.0$, the system is above the critical temperature of the KLS model, and we therefore have a single boundary between the homogenous phase and the two-species order. The behaviors of $S(0,1)$ and $\Delta(0,1)$ suggest that this boundary is continuous, though this hypothesis requires some analysis of larger systems before it can be taken seriously. Upon lowering T to 1.2, the system is below T_{KLS}, and therefore

at $f = 0$ we observe a transition of the KLS type as a function of E. Now the question arises: how large can we make f and still observe this transition? In our studies of this finite system we found this transition between $f = 0$ and $f = .04$. We also observed the parallel strip at $f = .05$, but here the system orders *first* into the *transverse strip*, and then upon increasing E further orders into the parallel strip. Similar behavior was observed at $f = .075$, though in this case the high E phase cannot be labeled precisely as an ordered phase in this finite system. At even higher f we observe only the transition into the transverse strip.

We have also presented in sec. 2.2.1 a phase diagram at fixed E, varying T and f. At high f we observe a continuous transition into the transverse strip as T is lowered, and we have also presented a rough scaling analysis of this transition. At smaller f ($.05 \leq f \leq .10$) we observe two transition as T is lowered: first into the transverse strip (continuous), and then into the parallel strip (1st order). And finally at small f a single transition is observed into the parallel strip (continuous). We have presented data for several system sizes in the vicinity of the junction of these three lines, where the boundaries apparently scale with the number of rows of the minority species which span the finite lattice. It is yet unclear what this result implies for the thermodynamic limit.

Several projects suggest themselves to extend this work. First, an analysis of larger systems at fixed T could answer some questions, especially regarding the fate of the 'competitive' phase. Many of the 'transitions' in the 40×40 system require an analysis of larger lattices in order to verify their existence. Second, an analysis of the KLS transition in the presence of disorder (i.e., a few minority charges) may reveal to what extent the transition is modified in the limit of small concentrations of the minority species.

Chapter 3

The Homogenous Phase

As we have mentioned in the introduction, power law correlations have been observed in the homogenous phase of both the KLS model[26] and the two-species model[31]. Thus, despite the *appearance* of disorder, there is some structure in the homogenous phase which we would like to uncover. We will investigate this behavior by measuring quantities sensitive to this structure, and comparing to the same quantities calculated from a continuum theory.

In this section, we will develop the continuum theory, which we use to investigate the homogenous phase. Since we would like to compute quantities which can be compared to simulation results, we consider coarse-grained versions of our microscopic variables: $\sigma(\mathbf{x}) \to \psi(\mathbf{x})$ and $n(\mathbf{x}) \to \rho(\mathbf{x})$. $\psi(\mathbf{x})$ is therefore the local 'charge' density, and $\rho(\mathbf{x})$ is the local mass density. If we consider two-point functions, there are three different quantities which can be formed: $G_{\rho\rho}(\mathbf{x}) \equiv \langle\rho(\mathbf{x})\rho(\mathbf{0})\rangle - \langle\rho(\mathbf{x})\rangle\langle\rho(\mathbf{0})\rangle$, $G_{\psi\psi}(\mathbf{x}) \equiv \langle\psi(\mathbf{x})\psi(\mathbf{0})\rangle - \langle\psi(\mathbf{x})\rangle\langle\psi(\mathbf{0})\rangle$, and $G_{\rho\psi}(\mathbf{x}) \equiv \langle\rho(\mathbf{x})\psi(\mathbf{0})\rangle - \langle\rho(\mathbf{x})\rangle\langle\psi(\mathbf{0})\rangle$. In fact, direct measurement of correlation functions in real-space is quite computationally expensive, requiring (L is the dimension of the lattice) $\mathcal{O}(L^4)$ operations for a two-point function. Instead, we consider the fourier transform of the two-point function, or structure factor, defined by $S_{\rho\rho}(\mathbf{k}) \equiv \sum_{\mathbf{x}} G_{\rho\rho}(\mathbf{x})e^{i\mathbf{kx}}$, and similarly for $S_{\psi\psi}(\mathbf{k})$ and $S_{\rho\psi}(\mathbf{k})$. For a particular $\mathbf{k}$, the structure factor requires only $\mathcal{O}(L^2)$ operations to compute. (Recall that $S_{\rho\rho}(\mathbf{k})$ was used in earlier sections as an order parameter, signalling the appearance of the two ordered phases, with $\mathbf{k} = (0, 2\pi/L_y)$ and $\mathbf{k} = (2\pi/L_x, 0)$.) Notice that $G_{\rho\rho}(\mathbf{x})$ and $G_{\psi\psi}(\mathbf{x})$ are even in $\mathbf{x}$, therefore $S_{\rho\rho}(\mathbf{k})$ and $S_{\psi\psi}(\mathbf{k})$ are strictly real. $G_{\rho\psi}(\mathbf{x})$, however, is odd in $\mathbf{x}$, and therefore will in general be complex.

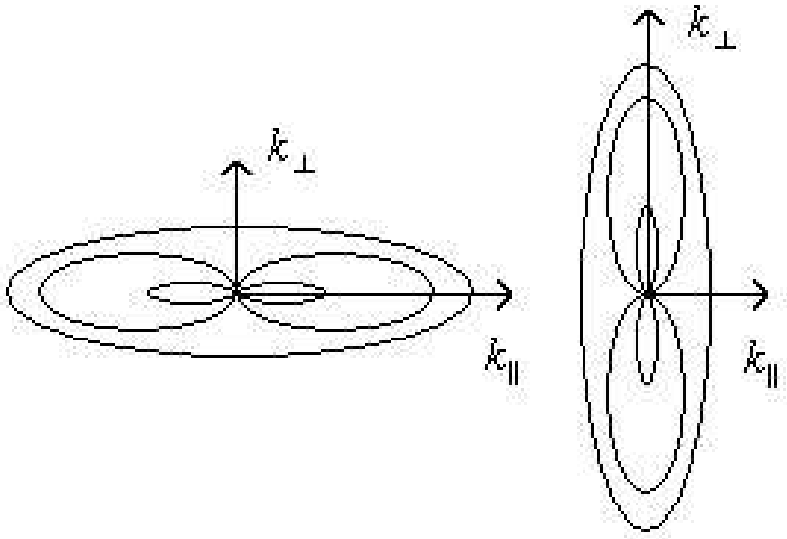

Figure 3.1: Contour plot sketches of structure factors for the SHZ (left) and KLS (right) systems.

The effective long-range interactions are notable in these models because they are dynamically generated; both the interactions and the dynamics are short-ranged. However, the nature of the correlations is quite different in the two models. This difference is evidenced profoundly by the behavior of the structure factor, sketched in fig. 3.1. In each case there is a discontinuity singularity at the origin, which is characterized by the ratio $R \equiv \lim_{k_\parallel \to 0} S(k_\perp = 0, k_\parallel) / \lim_{k\perp \to 0} S(k_\perp, k_\parallel = 0)$. (As a reminder, $k_{\parallel(\perp)}$ means components of k parallel(perpendicular) to E.) In the two-species case, the structure factor is non-monotonic in $k_\parallel$ for small $k_\perp$, while in the KLS case this situation is reversed. The difference reflects the different mechanisms by which correlations build in each case.

In our model, changing the fraction f of the minority species interpolates between the KLS and the two-species models. It is then interesting to wonder: how do the long-range correlations behave as a function of f? This will be the main thrust of our investigations in this chapter. We will develop linearized equations of motion for the local charge and particle densities. The short-wavelength, fast degrees of freedom which are lost in the (phenomenological) coarse-graining process will be modeled by a noise term. Solutions will be found for the local densities, and structure factors will be computed

by forming products of these solutions and averaging over the noise. We will then compare the results of the calculation to the simulation results.

3.1 Equations of Motion

We begin by writing down mesoscopic equations of motion for the local densities of positive ($\rho^+(\mathbf{x},t)$) and negative ($\rho^-(\mathbf{x},t)$) particles. Though these equations can be derived from a master equation[36], we simply postulate them on the basis of symmetries:

$$\begin{aligned}\partial_t\rho^+(\mathbf{x},t) &= \boldsymbol{\nabla}\boldsymbol{\Gamma}\left(\varphi(\mathbf{x},t)\,\boldsymbol{\nabla}\rho^+(\mathbf{x},t) - \rho^+(\mathbf{x},t)\,\boldsymbol{\nabla}\varphi(\mathbf{x},t)\right) \qquad (3.1)\\ &\quad -\mathcal{E}\nabla_\parallel\varphi(\mathbf{x},t)\,\rho^+(\mathbf{x},t)\\ \partial_t\rho^-(\mathbf{x},t) &= \boldsymbol{\nabla}\boldsymbol{\Gamma}\left(\varphi(\mathbf{x},t)\,\boldsymbol{\nabla}\rho^-(\mathbf{x},t) - \rho^-(\mathbf{x},t)\,\boldsymbol{\nabla}\varphi(\mathbf{x},t)\right) \qquad (3.2)\\ &\quad +\mathcal{E}\nabla_\parallel\varphi(\mathbf{x},t)\,\rho^-(\mathbf{x},t)\end{aligned}$$

The first part ($\boldsymbol{\nabla}\boldsymbol{\Gamma}$...) describes unbiased diffusion of the + and − densities, with diffusion matrix $\boldsymbol{\Gamma}$; $\varphi = 1-\rho^+-\rho^-$ is the local density of holes.[1] In order to allow for the effects of anisotropy, $\boldsymbol{\Gamma}$ is diagonal, but distinguishes the subspaces parallel and perpendicular to E, and is therefore *not* proportional to the unit matrix. The second part describes the ohmic current induced by the (coarse-grained) hopping bias $\mathcal{E}$. The subscript $\parallel$ is used to indicate the subspace parallel to $\mathcal{E}$; note that $\mathcal{E}$ couples only to the '$\parallel$' gradient. It is convenient to rewrite this pair of equations as equations of motion for the local particle ($\rho \equiv \rho^+ + \rho^-$) and charge ($\psi \equiv \rho^+ - \rho^-$) densities, as we measure correlations of these quantities in simulations. To keep things simple, we consider only small fluctuations about the mean densities, which ought to suffice for describing the homogenous phase. Thus, we write $\rho = 1/2 + \rho$, and $\psi = Q + \psi$, (ρ and ψ are now understood to be the *fluctuations*) and consider only terms linear in ρ and ψ. The average particle density is fixed at $1/2$, and the average charge density is written Q, $Q \equiv (N_+ - N_-)/L_xL_y$,where $N_{+(-)}$ is the total number of positive (negative) particles. We note that Q carries the same information as f, though $Q = 0$ corresponds to $f = .5$, and

[1] We will use **bold** to indicate vectors and matrices.

$Q = .5$ corresponds to $f = 0$. The linearized equations are:

$$\begin{aligned} \partial_t \rho(\mathbf{x},t) &= \boldsymbol{\nabla}\boldsymbol{\Gamma}\boldsymbol{\nabla}\rho(\mathbf{x},t) - \mathcal{E}\nabla_\parallel\left(\frac{1}{2}\psi(\mathbf{x},t) - Q\rho(\mathbf{x},t)\right) \\ &\quad -\boldsymbol{\nabla}\left(\boldsymbol{\eta}^+(\mathbf{x},t) + \boldsymbol{\eta}^-(\mathbf{x},t)\right) \end{aligned} \tag{3.3}$$

$$\begin{aligned} \partial_t \psi(\mathbf{x},t) &= \frac{1}{2}\boldsymbol{\nabla}\boldsymbol{\Gamma}\boldsymbol{\nabla}\psi(\mathbf{x},t) + Q\boldsymbol{\nabla}\boldsymbol{\Gamma}\boldsymbol{\nabla}\rho(\mathbf{x},t) \\ &\quad -\boldsymbol{\nabla}\left(\boldsymbol{\eta}^+(\mathbf{x},t) - \boldsymbol{\eta}^-(\mathbf{x},t)\right) \end{aligned} \tag{3.4}$$

We have introduced noise terms $\boldsymbol{\eta}^+$ and $\boldsymbol{\eta}^-$ to model the fast degrees of freedom which have been lost through the coarse-graining procedure. These are the noises associated with ρ^+ and ρ^-, and so their sum and difference appear in the equations for ρ and ψ. The noise is delta-correlated with zero average:

$$\langle \eta_i^\alpha \rangle = 0 \tag{3.5}$$

$$\left\langle \eta_i^\alpha(\mathbf{x},t)\,\eta_j^\beta\left(\mathbf{x}',t'\right)\right\rangle = 2\delta^{\alpha\beta}\sigma_{ij}^\alpha\delta\left(\mathbf{x}-\mathbf{x}'\right)\delta\left(t-t'\right) \tag{3.6}$$

The superscript refers to the charge index (+ or −), and the subscript refers to the spatial index. We assume that the noise correlation matrix σ_{ij}^α is diagonal, and proportional to the identity matrix in the transverse subspace. As in the case of $\boldsymbol{\Gamma}$, allowing different noise correlations in the two subspaces accounts for the possible effects of anisotropy. Although one may have anisotropic $\boldsymbol{\Gamma}$ and σ_{ij}^α in equilibrium systems, one always has $\boldsymbol{\Gamma} \propto \sigma_{ij}^\alpha$ by virtue of the Fluctuation-Dissipation Theorem (FDT). Here we are not constrained by FDT, and in general $\boldsymbol{\Gamma}$ is not proportional to σ_{ij}^α.

In Fourier space these quations take a particularly simple form, thanks to translational invariance. We therefore define the transforms, e.g., for $\rho(\mathbf{x},t)$:

$$\rho(\mathbf{x},t) \equiv \int \frac{d\omega}{2\pi}\int \frac{d^dk}{(2\pi)^d}\rho(\mathbf{k},\omega)\,e^{i(\mathbf{k}\cdot\mathbf{x}-\omega t)} \tag{3.7}$$

The solution is then found:

$$\begin{pmatrix} \rho(\mathbf{k},\omega) \\ \psi(\mathbf{k},\omega) \end{pmatrix} = -i\mathbf{k}\left[\mathbb{L}(\mathbf{k}) - i\omega\mathbb{I}\right]^{-1}\begin{pmatrix} \boldsymbol{\eta}^+(\mathbf{k},\omega) + \boldsymbol{\eta}^-(\mathbf{k},\omega) \\ \boldsymbol{\eta}^+(\mathbf{k},\omega) - \boldsymbol{\eta}^-(\mathbf{k},\omega) \end{pmatrix} \tag{3.8}$$

where $\mathbb{I}$ is the identity matrix, and the matrix $\mathbb{L}(\mathbf{k})$ is given by:

$$\mathbb{L}(\mathbf{k}) = \begin{pmatrix} \mathbf{k}\boldsymbol{\Gamma}\mathbf{k} + i\mathcal{E}Qk_\parallel & -\frac{i}{2}\mathcal{E}k_\parallel \\ -Q\mathbf{k}\boldsymbol{\Gamma}\mathbf{k} & -\frac{1}{2}\mathbf{k}\boldsymbol{\Gamma}\mathbf{k} \end{pmatrix} \tag{3.9}$$

From this solution we compute the structure factors by forming products, e.g. $S_{\rho\rho}(\mathbf{k},\omega) = \langle \rho(\mathbf{k},\omega)\rho(-\mathbf{k},-\omega)\rangle$ (the average is over the noise), and by integrating over ω the equal-time structure factor is computed. Additionally, since the matrix $\mathbb{L}(\mathbf{k}) - i\omega\mathbb{I}$ contains only the linear terms from the equations of motion, the behavior of its eigenvalues $\omega(\mathbf{k})$ will contain information about the stability of the homogenous phase with respect to small perturbations.

3.1.1 Structure Factors

Before computing the structure factors, we consider the stability of the homogenous phase with respect to small perturbations. Specifically, we consider solutions of eg. (3.3) which are of the form

$$\rho(\mathbf{x},t) = \rho_0 + \int \frac{d^dk}{(2\pi)^d}\rho\left(\mathbf{k},t\right)e^{i(\mathbf{k}\cdot\mathbf{x}-\omega(\mathbf{k})t)} \tag{3.10}$$

$$\psi(\mathbf{x},t) = \psi_0 + \int \frac{d^dk}{(2\pi)^d}\psi\left(\mathbf{k},t\right)e^{i(\mathbf{k}\cdot\mathbf{x}-\omega(\mathbf{k})t)} \tag{3.11}$$

Neglecting the noise terms for the moment, the linear theory takes the form:

$$i\omega\left(\mathbf{k}\right)\boldsymbol{\xi}\left(\mathbf{k},\omega\right) = \mathbb{L}\left(\mathbf{k}\right)\boldsymbol{\xi}\left(\mathbf{k},\omega\right) \tag{3.12}$$

where we have written $\boldsymbol{\xi}(\mathbf{k},t)$ for the vector with components $\rho(\mathbf{k},t)$ and $\psi(\mathbf{k},t)$. Aside from the trivial solution $\boldsymbol{\xi}(\mathbf{k},\omega) = 0$, the eigenvalues $\omega(\mathbf{k})$ are determined by the condition: $\det[\mathbb{L}(\mathbf{k}) - i\omega\mathbb{I}] = 0$. Solving for the eigenvalues of $\mathbb{L}$ yields:

$$i\omega(\mathbf{k}) = \begin{cases} \mathbf{k}\boldsymbol{\Gamma}\mathbf{k} \\ -i\mathcal{E}k_{\|}Q + \frac{1}{2}\mathbf{k}\boldsymbol{\Gamma}\mathbf{k} \end{cases} \tag{3.13}$$

The $\mathrm{Re}(i\omega(\mathbf{k}))$ is always ≥ 0. Thus the homogenous phase is stable for all $\mathbf{k}$. Of course, the results are not inconsistent with the observation of phase separation in simulations, as here we are interested in the homogenous phase and have therefore considered only small fluctuations.

In order to compute structure factors, we compute products of the solutions in the frequency domain, such as $\rho(\mathbf{k},\omega)\rho(\mathbf{k}',\omega')$, and then average over the noise. We then transform back to the time domain to consider equal-time correlations, as measured in simulations. Notice that when forming the

products, we will encounter two different combinations of $\boldsymbol{\eta}^+$ and $\boldsymbol{\eta}^-$:

$$\begin{aligned}\left\langle \left[\eta_i^+(\mathbf{k},\omega) \pm \eta_i^-(\mathbf{k},\omega)\right]\left[\eta_j^+(\mathbf{k}',\omega') \pm \eta_j^-(\mathbf{k}',\omega')\right]\right\rangle &= \qquad (3.14)\\ &= 2\sigma_{ij}^S\delta(\mathbf{k}+\mathbf{k}')\delta(\omega+\omega')\\ \left\langle \left[\eta_i^+(\mathbf{k},\omega) \pm \eta_i^-(\mathbf{k},\omega)\right]\left[\eta_j^+(\mathbf{k}',\omega') \mp \eta_j^-(\mathbf{k}',\omega')\right]\right\rangle &= \qquad (3.15)\\ &= 2\sigma_{ij}^A\delta(\mathbf{k}+\mathbf{k}')\delta(\omega+\omega')\end{aligned}$$

where we have introduced the matrices $(\sigma_{ij}^+ + \sigma_{ij}^-) \equiv \sigma_{ij}^S$ and $(\sigma_{ij}^+ - \sigma_{ij}^-) \equiv \sigma_{ij}^A$ for, respectively, the symmetric and antisymmetric combinations of the ρ^+ and ρ^- noises. The structure factors, $S(\mathbf{k},\omega)$ are then of the form:

$$S_{ab}(\mathbf{k},\omega) = \frac{\mathbf{k}\boldsymbol{\sigma}^S\mathbf{k}F_{ab}^S(\mathbf{k},\omega) + \mathbf{k}\boldsymbol{\sigma}^A\mathbf{k}F_{ab}^A(\mathbf{k},\omega)}{\det\left[\mathbb{L}(\mathbf{k}) - i\omega\mathbb{I}\right]\det\left[\mathbb{L}(-\mathbf{k}) + i\omega\mathbb{I}\right]} \qquad (3.16)$$

where the functions $F^S(\mathbf{k},\omega)$ and $F^A(\mathbf{k},\omega)$ are combinations of the matrix elements of $\mathbb{L}(\mathbf{k}) - i\omega\mathbb{I}$ to be listed below, and the indices ab refer to the densities from which the structure factor is formed. In simulations, we measure the *equal-time* structure factor, $S_{ab}(\mathbf{k})$. We therefore need to transform back into the time domain by integrating over ω. The zeros of $\det[\mathbb{L}(\mathbf{k}) - i\omega\mathbb{I}]$ are the eigenvalues $\omega(\mathbf{k})$ computed above (both lie below the real axis), and the zeros of $\det[\mathbb{L}(-\mathbf{k}) + i\omega\mathbb{I}]$ are the mirror images above the real axis. Carrying out the contour integration yields an expression for $S_{ab}(\mathbf{k}, t-t') = \langle a(\mathbf{k},t)b(\mathbf{k},t')\rangle$, and setting $t = t'$ gives the equal-time structure factors. Each is of the form:

$$S_{ab}(\mathbf{k}) = \frac{2\pi\left(\mathbf{k}\sigma^S\mathbf{k}F_{ab}^S(\mathbf{k}) + \mathbf{k}\sigma^A\mathbf{k}F_{ab}^A(\mathbf{k})\right)}{D(\mathbf{k})} \qquad (3.17)$$

with the same denominator $D(\mathbf{k})$

$$D(\mathbf{k}) = \mathbf{k}\boldsymbol{\Gamma}\mathbf{k}\left(\frac{9}{4}(\mathbf{k}\boldsymbol{\Gamma}\mathbf{k})^2 + Q^2\left(\mathcal{E}k_\parallel\right)^2\right)\left(\frac{1}{4}(\mathbf{k}\boldsymbol{\Gamma}\mathbf{k})^2 + Q^2\left(\mathcal{E}k_\parallel\right)^2\right) \qquad (3.18)$$

and different functions $F^S_{ab}(\mathbf{k})$ and $F^A_{ab}(\mathbf{k})$:

$$F^S_{\rho\rho}(\mathbf{k}) = \tag{3.19}$$
$$= \frac{9}{16}(\mathbf{k\Gamma k})^4 + \left(\frac{11}{4}Q^2 + \frac{3}{16}\right)(\mathbf{k\Gamma k})^2\left(\mathcal{E}k_\parallel\right)^2 + \left(\frac{3}{4}Q^2 + 2Q^4\right)\left(\mathcal{E}k_\parallel\right)^4$$
$$F^A_{\rho\rho}(\mathbf{k}) = -Q\left(\mathcal{E}k_\parallel\right)^2\left(2Q^2\left(\mathcal{E}k_\parallel\right)^2 + \frac{1}{2}(\mathbf{k\Gamma k})^2\right) \tag{3.20}$$
$$F^S_{\psi\psi}(\mathbf{k}) = \tag{3.21}$$
$$= \frac{3}{4}(\mathbf{k\Gamma k})^4\left(Q^2 + \frac{3}{4}\right) + \left(3Q^4 + \frac{19}{4}Q^2\right)(\mathbf{k\Gamma k})^2\left(\mathcal{E}k_\parallel\right)^2 + Q^4\left(\mathcal{E}k_\parallel\right)^4$$
$$F^A_{\psi\psi}(\mathbf{k}) = -2Q(\mathbf{k\Gamma k})^2\left(\frac{3}{4}(\mathbf{k\Gamma k})^2 + 3Q^2\left(\mathcal{E}k_\parallel\right)^2\right) \tag{3.22}$$
$$\mathrm{Re}F^S_{\rho\psi}(\mathbf{k}) = \tag{3.23}$$
$$= Q\left[\frac{3}{8}(\mathbf{k\Gamma k})^4 + \left(\frac{3}{2}Q^2 - \frac{1}{8}\right)(\mathbf{k\Gamma k})^2\left(\mathcal{E}k_\parallel\right)^2 - \frac{1}{2}Q^2\left(\mathcal{E}k_\parallel\right)^4\right]$$
$$\mathrm{Im}F^S_{\rho\psi}(\mathbf{k}) = \tag{3.24}$$
$$= \mathcal{E}k_\parallel(\mathbf{k\Gamma k})\left[\left(\frac{1}{2}Q^2 + \frac{3}{8}\right)(\mathbf{k\Gamma k})^2 + \left(\frac{3}{2}Q^2 + 2Q^4\right)\left(\mathcal{E}k_\parallel\right)^2\right]$$
$$\mathrm{Re}F^A_{\rho\psi}(\mathbf{k}) = -3(\mathbf{k\Gamma k})^2\left[\frac{1}{4}(\mathbf{k\Gamma k})^2 + Q^2\left(\mathcal{E}k_\parallel\right)^2\right] \tag{3.25}$$
$$\mathrm{Im}F^A_{\rho\psi}(\mathbf{k}) = Q\left(\mathcal{E}k_\parallel\right)(\mathbf{k\Gamma k})\left[(\mathbf{k\Gamma k})^2 + 4Q^2\left(\mathcal{E}k_\parallel\right)^2\right] \tag{3.26}$$

3.2 Monte Carlo Results

In order to compare the results of the calculation with data from simulations, the structure factors $S_{ab}(\mathbf{k})$ were measured for a range of Q in a 100×100 system. The larger system gives a better resolution for the small-k behavior, without incurring much of an increase in running time since we are well above T_c. The definition of the structure factors, as *measured* in simulations, has already been given earlier. However, when we used the structure factors as order parameters, we were only interested in the particle correlations, i.e., the presence or absence of a strip of higher density. Here, we are interested in correlations of particles with particles ($S_{\rho\rho}(\mathbf{k})$), correlations of charges with charges ($S_{\psi\psi}(\mathbf{k})$), and correlations of particles with charges ($S_{\rho\psi}(\mathbf{k})$). As a

reminder, we have two variables which specify the occupation of the lattice. $n(\mathbf{x}) = 1$ or 0 for a particle of either type or a hole, and $\sigma(\mathbf{x}) = +(-)1$ or 0 for a positive (negative) particle or hole. The structure factors as measured in simulations are then defined:

$$S^{obs}_{\rho\rho}(\mathbf{k}) \equiv \left\langle \frac{\pi}{L_x L_y} \sum_{\mathbf{x},\mathbf{x}'} n(\mathbf{x}) n(\mathbf{x}') e^{2\pi i \mathbf{k}\cdot(\mathbf{x}-\mathbf{x}')} \right\rangle \tag{3.27}$$

$$S^{obs}_{\psi\psi}(\mathbf{k}) \equiv \left\langle \frac{\pi}{L_x L_y} \sum_{\mathbf{x},\mathbf{x}'} \sigma(\mathbf{x}) \sigma(\mathbf{x}') e^{2\pi i \mathbf{k}\cdot(\mathbf{x}-\mathbf{x}')} \right\rangle \tag{3.28}$$

$$S^{obs}_{\rho\psi}(\mathbf{k}) \equiv \left\langle \frac{\pi}{L_x L_y} \sum_{\mathbf{x},\mathbf{x}'} n(\mathbf{x}) \sigma(\mathbf{x}') e^{2\pi i \mathbf{k}\cdot(\mathbf{x}-\mathbf{x}')} \right\rangle \tag{3.29}$$

The superscript 'obs' is a reminder that these are observed quatities, to be compared with the calculated values. Though in the introduction to this section, we defined $G_{ab}(\mathbf{x})$ as the *truncated* two-point function, here we have not subtracted the (one-point) averages. This will not be an issue here, as we are considering only $T > T_c$, where all averages of the type $\langle n_{\mathbf{k}} \rangle \equiv \langle \sum_{\mathbf{x}} n(\mathbf{x}) e^{2\pi i \mathbf{k}\cdot\mathbf{x}} \rangle$ (and the analagous quantity $\langle \sigma_{\mathbf{k}} \rangle$) are $\mathcal{O}(1/L^2)$, except of course for $\langle n_{\mathbf{k}=\mathbf{0}} \rangle$ which is trivially related to the average density. After allowing $2.0 \times (10^5)$ MCS for the system to reach a steady-state, the above quantities are measured every 800 MCS for the next $1.6 \times (10^6)$ MCS. The results of three such runs are then averaged together.

In the next section, we look at the structure factors for $Q = 0$, which corresponds to equal numbers of each type of particle. We then turn to the $Q \neq 0$ case.

3.2.1 Q = 0

The $Q = 0$ case has been extensively studied before. Korniss carried out a similar analysis of structure factors, allowing for charge exchange and average density away from half-filling[37]. However, the analysis was carried through in different variables, the density of + and −, rather than their sum and difference. Here, we look to see how the measured quantities are affected by the change of variable, and compare to the earlier results. This will provide a reference for our analysis of the $Q \neq 0$ case.

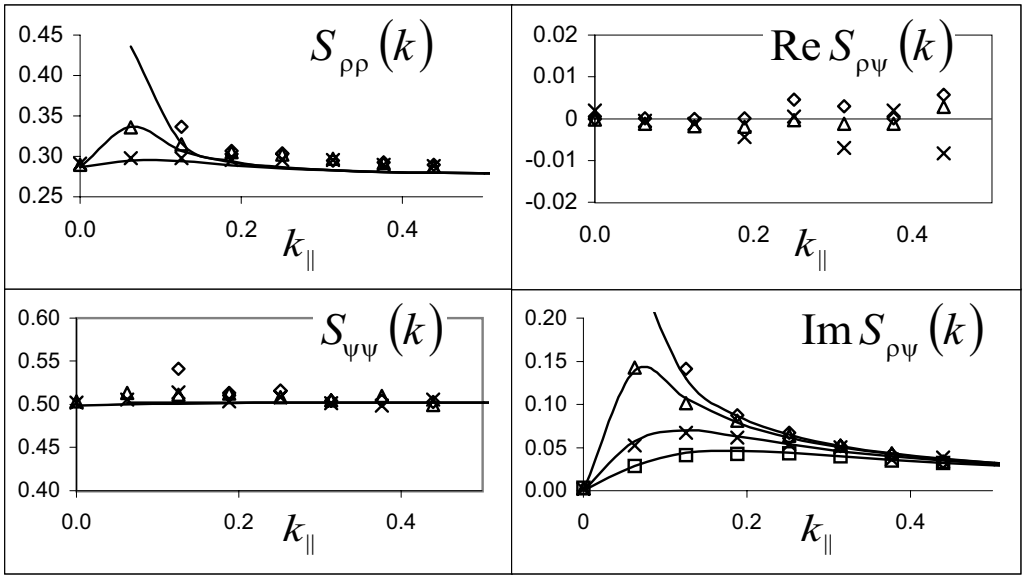

Figure 3.2: $Q = 0$ structure factors as a function of $k_{\|}$ for different $k_{\perp}$. $k_{\perp} = 2\pi m/L_x$, with $m = 0$ (diamonds), $m = 1$ (triangles), $m = 2$ ($\times$'s), $m = 3$ (squares). The solid line indicates the fit to eqs (3.30 - 3.34).

When $Q = 0$, eqs. (3.18 - 3.26) simplify to:

$$D(\mathbf{k}) = \frac{9}{16}\mathbf{k\Gamma k}^5 \tag{3.30}$$

$$F^S_{\rho\rho}(\mathbf{k}) = \frac{9}{16}(\mathbf{k\Gamma k})^4 + \frac{3}{16}(\mathbf{k\Gamma k})^2\left(\mathcal{E}k_{\|}\right)^2 \tag{3.31}$$

$$F^S_{\psi\psi}(\mathbf{k}) = \frac{9}{16}(\mathbf{k\Gamma k})^4 \tag{3.32}$$

$$\mathrm{Re}F^S_{\rho\psi}(\mathbf{k}) = 0 \tag{3.33}$$

$$\mathrm{Im}F^S_{\rho\psi}(\mathbf{k}) = \frac{3}{8}\mathcal{E}k_{\|}(\mathbf{k\Gamma k})^3 \tag{3.34}$$

where we have also set the elements of $\boldsymbol{\sigma}^A = \mathbf{0}$. Fig. 3.2 shows the structure factors at $E/T = .16$, well below the critical value $E/T_c = .24$. The measured values are indicated by the symbols; lines correspond to the fit to eq. (3.17).

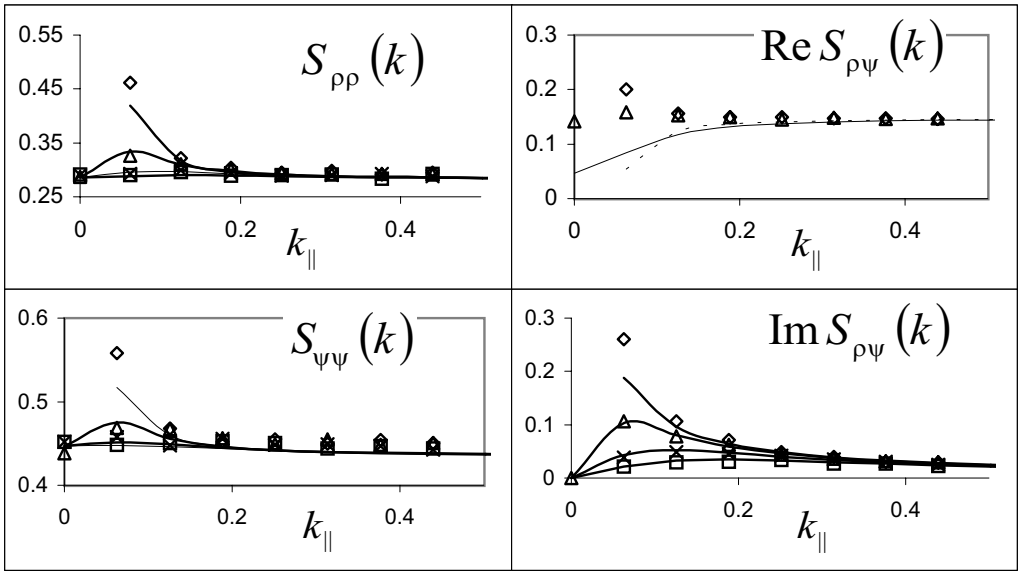

Figure 3.3: $Q = .25$ structure factors as a function of $k_{\|}$ for different $k_{\perp}$. Symbols same as in fig. 3.2. The solid line indicates the fit to eqs. (3.18 - 3.26), with $\boldsymbol{\sigma}^A = \mathbf{0}$.

In the remainder of this work, we take $\boldsymbol{\sigma}^A = \mathbf{0}$, which reduces the number of fit parameters which need to be considered. Physically, this amounts to assuming that $\rho^+(\mathbf{x}, t)$ and $\rho^-(\mathbf{x}, t)$ experience the same noise. Though we must bear this assumption in mind, it is probably reasonable so long as ρ^+ and ρ^- are nearly equal.

The data were fitted qualitatively, by adjusting the parameters and attempting to optimize the fit for all 4 structure factors, and for each different $\mathbf{k}$ simultaneously. We stress that the optimization was not quantitative, a more rigorous study would conduct a more systematic search of the parameter space and assess the quality of the fit by minimization of an appropriate error function. Nevertheless, the qualitative fit a) demonstrates that the mesoscopic description is *consistent* with the data, and b) allows us to estimate some key parameters: $\sigma_{\perp}/\Gamma_{\perp} = .046(2)$, $\sigma_{\|}/\Gamma_{\|} = .042(2)$, $\mathcal{E}/\Gamma_{\|} = .083(1)$.

The best fit for each different $S_{ab}(\mathbf{k})$ corresponds to a slightly different set of the parameters; this is how the errors were estimated. Notice that the non-monotonic character of $S(\mathbf{k})$ is most visible in the $\mathrm{Im}S_{\rho\psi}(\mathbf{k})$. This is apparently an artifact of the choice of variables; similar quantities formed from the $\rho^+(\mathbf{x},t)$ and $\rho^-(\mathbf{x},t)$ variables are more sensitive to this structure[37]. Also, we note that $\mathrm{Re}S_{\rho\psi}$ is zero, apart from fluctuations, as predicted by the calculation. Since the $\mathrm{Re}S_{\rho\psi}$ comes from the even parts of

3.2.2 Nonzero Q

Now we look to see what changes when we move away from $Q = 0$. A glance at eqs. (3.19 - 3.26) shows that nonzero Q will not introduce any extra parameters (aside from Q itself), but only modifies some of the constants which multiply factors of $\mathbf{k\Gamma k}$ and $\mathcal{E}k_\parallel$. (We still assume $\boldsymbol{\sigma}^A = \mathbf{0}$). We would therefore like to see whether the data can again be fitted to a single set of fit parameters, which works for each $S_{ab}(\mathbf{k})$. In fig. 3.3 are plotted the data and the fits for each $S_{ab}(\mathbf{k})$. First, note that the data for $\mathrm{Re}S_{\rho\psi}(\mathbf{k})$ do not fit the theoretical curve at small $\mathbf{k}$. Furthermore, it was not possible to fit all four S's with a single set of fit parameters. For example, the best fit for $S_{\psi\psi}(\mathbf{k})$ is given by $\sigma_\perp/\Gamma_\perp = .044$, while for $\mathrm{Im}S_{\rho\psi}(\mathbf{k}y)$ $\sigma_\perp/\Gamma_\perp = .019$ was used. These values are typical of the variation in fit parameters between different S's. The results probably indicate the failure of an assumption which was made in developing the theoretical description. It seems likely that the assumption which was made regarding the noise experienced by the ρ^+ and ρ^- densities is breaking down. Apparently, when $Q \neq 0$, the antisymmetric combination (see eq. (3.15)) of the noises ($\boldsymbol{\sigma}^A$) is no longer vanishing. In principle, one could return to the theoretical descriptions (3.19 - 3.26) and fit the data with $\boldsymbol{\sigma}^A \neq \mathbf{0}$. However, there are already 5 adjustable parameters in the simplified description, and taking $\boldsymbol{\sigma}^A \neq \mathbf{0}$ will introduce an additional 2. We defer a further discussion of this issue to the summary chapter, where we will discuss possibilities for further research.

3.3 Summary

We have developed a theoretical description of the homogenous phase, based on linearized equations of motion for the local densities. Expressions for the structure factors were computed from the solutions to the equations of mo-

tion. The theoretical expressions display the expected characteristics, namely the nonmonotonic structure and small **k** singularity, which captures the violation of the FDT and the long-range correlations. The theoretical expressions were then fitted to the data, under the assumption that the antisymmetric part of the noise correlations vanishes. This assumption apparently fails when $Q \neq 0$, suggesting that further work is needed. In particular, one could fit the full expressions, including the antisymmetric part of the noise, to the observed S's. It would be advisable to carry out the data-fitting in a more quantitative way, by constructing a function which characterizes the error. This would not only provide rigorous error bars on the fitted values, but would also give a sense of how sensitive the fit is to the different parameters. For example, a 10% change in one parameter may not affect the fit very much, while a 10% change in some other parameter may ruin the fit. This information would be quite useful, as it would give an idea about which of the theoretical parameters are most crucial.

Chapter 4

Three Point Correlations

In this section, we will look at an interesting feature of the KLS model, namely the effect of the hopping bias on higher order correlation functions. In the *equilibrium* Ising model, symmetry under charge (C) ($\sigma(\mathbf{r}) \to -\sigma(\mathbf{r})$, where $\sigma(\mathbf{r})$ is the spin at site $\mathbf{r}$) and parity (P) ($y \to -y$) transformations is separately preserved. Any correlation of an odd number of σ's is odd under C. However, all such correlation functions must be even under P, and we see that any correlation of an odd number of σ's must vanish. In the KLS model, on the other hand, the hopping bias couples to the charge and breaks the symmetry in P, so that only transformations under the combined operation CP leave the model invariant. Since correlations of an odd number of σ's are symmetric under the *combined* operation CP, we see that such correlations are in general different from zero. In this section, we will examine the behavior of the simplest of these correlation functions, namely the three point function: $G(\mathbf{r}, \mathbf{r}') \equiv \langle \sigma(\mathbf{r})\sigma(\mathbf{r}')\sigma(\mathbf{0}) \rangle$. We first consider the field theory for the KLS model, to see what sort of behavior should be expected of G. We then turn to simulations, in order to see whether the observed behavior is consistent with the field theory. We conclude with some interesting possibilities for further investigation.

4.1 Continuum Description

In this section, we briefly discuss the continuum field theory which is used to compute the three-point function perturbatively. We are only reviewing the salient points here, more detailed discussion of the KLS field theory[24]

and the three-point function calculation[38] have been published elsewhere. The outline of the procedure is as follows: a Langevin equation is developed for the magnetization, $\phi(\mathbf{r})$. $\phi(\mathbf{r})$ is the local magnetisation at site $\mathbf{r}$, which represents the microscopic spins in the neighborhood of $\mathbf{r}$ after coarse graining. In the spirit of phenomenological studies of critical dynamics, we simply postulate the following Langevin equation on the basis of symmetries:

$$\begin{aligned}\frac{\partial\phi(\mathbf{r},t)}{\partial t} = & \lambda\left[\boldsymbol{\nabla}^2\left(\tau_\perp - \kappa_\perp\boldsymbol{\nabla}^2\right)\phi + \partial^2\left(\tau_\parallel - \kappa_\parallel\partial^2\right)\phi - \kappa_\times\boldsymbol{\nabla}^2\partial^2\phi\right] \\ & +\left(u_\perp\boldsymbol{\nabla}^2 + u_\parallel\partial^2\right)\phi^3/3! + \mathcal{E}\partial\phi^2 - (\boldsymbol{\nabla}\cdot\boldsymbol{\xi} + \partial\zeta)\end{aligned} \tag{4.1}$$

The Langevin equation is based on the LGW Hamiltonian, though now we have a new nonlinearity associated with the bias, $\mathcal{E}$. We also (as in sec. 3.1) allow for the bias to split couplings, gradients and noises into directions parallel($\parallel$) and transverse ($\perp$)to the bias. Thus, $\tau\boldsymbol{\nabla}^2\phi^2 \to (\tau_\perp\boldsymbol{\nabla}_\perp^2 + \tau_\parallel\partial^2)\phi^2$,and ∂ ($\boldsymbol{\nabla}$) is now the gradient operator parallel (transverse) to the bias. The (anisotropic) noises have zero average and delta correlations:

$$\begin{aligned}\langle\boldsymbol{\nabla}\cdot\boldsymbol{\xi}(\mathbf{r},t)\,\boldsymbol{\nabla}'\cdot\boldsymbol{\xi}(\mathbf{r}',t')\rangle &= -2\eta_\perp\boldsymbol{\nabla}^2\delta(\mathbf{r}-\mathbf{r}')\,\delta(t-t') \\ \langle\partial\zeta(\mathbf{r},t)\,\partial'\zeta(\mathbf{r}',t')\rangle &= -2\eta_\parallel\partial^2\delta(\mathbf{r}-\mathbf{r}')\,\delta(t-t')\end{aligned} \tag{4.2}$$

Correlation functions are most easily computed by first reformulating the Langevin equation as a dynamic functional, $\mathcal{J}$, by introducing a Martin-Siggia-Rose response field[39], $\widetilde{\phi}(\mathbf{r})$. For our model,

$$\mathcal{J}\left(\phi,\widetilde{\phi}\right) = \int d^dr dt\left\{\widetilde{\phi}\left[\partial_t\phi - F(\phi)\right] + \eta_\parallel\widetilde{\phi}\partial^2\widetilde{\phi} + \eta_\perp\widetilde{\phi}\boldsymbol{\nabla}^2\widetilde{\phi}\right\} \tag{4.3}$$

where $F(\phi)$ is the systematic part of the Langevin equation, eq. (4.1). The exponential of $\mathcal{J}$ is then the statistical weight of a particular configuration of the fields ϕ and $\widetilde{\phi}$, performing the same role that βH would in equilibrium, and correlation functions are computed by taking appropriate derivatives of the exponential of $\mathcal{J}$. In practice, the derivatives must be computed perturbatively, by expanding the exponential in the nonlinearity $\mathcal{E}$. To first order in $\mathcal{E}$, the three-point correlation function in momentum space is

$$\begin{aligned}G(\mathbf{k}_1,\mathbf{k}_2,\mathbf{k}_3) = \frac{-2i\mathcal{E}\delta(\mathbf{k}_1+\mathbf{k}_2+\mathbf{k}_3)}{\Lambda(\mathbf{k}_1)+\Lambda(\mathbf{k}_2)+\Lambda(\mathbf{k}_3)}\big\{& k_{1\parallel}S(\mathbf{k}_2)\,S(\mathbf{k}_3) \\ & +\textit{cyclic permutations}\big\}\end{aligned} \tag{4.4}$$

where $S(\mathbf{k})$ is the two-point function, and $\Lambda(\mathbf{k}) = \tau_\parallel k_\parallel^2 + \tau_\perp k_\perp^2 + \kappa_\parallel k_\parallel^4 + \kappa_\times k_\parallel^2 k_\perp^2 + \kappa_\perp k_\perp^4$. Notice that G is odd under a reflection in y, and purely imaginary.

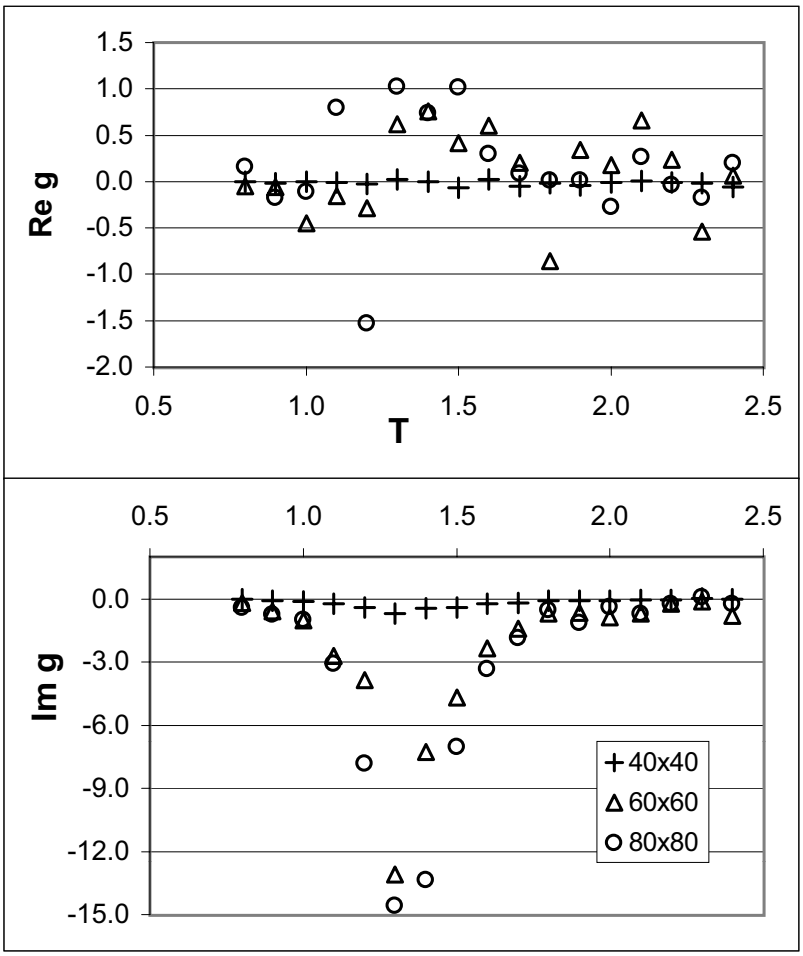

Figure 4.1: Reg and Img as a function of T at $E = 5.0$ for three system sizes.

4.2 Simulation Results

We have measured G in simulations (in dimension 2) in order to test these predictions. Hwang, et al have measured G in the KLS system before[38], here we extend the results by looking at system size dependence and several different bias strengths. Typical runs last $2M$ Monte Carlo steps (MCS), with $.2M$ MCS discarded to allow the system to reach steady-state. We allow $1,000$ MCS between measurements to ensure that consecutive measurements are not correlated. We do not measure the full $G(\mathbf{k}_1, \mathbf{k}_2, \mathbf{k}_3)$, as this would require $\mathcal{O}(L^4)$ computer time. Instead, we choose particular $\mathbf{k}$'s which are most sensitive to the nonequilibrium character of eq. (4.5). Specifically, we choose one of the momenta ($\mathbf{k}_1$, say) parallel to the bias, and one

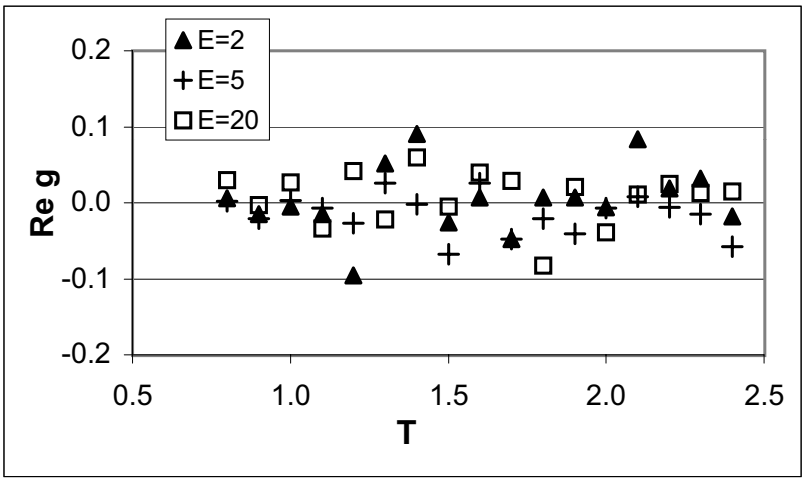

Figure 4.2: Reg as a function of T for various E.

transverse ($\mathbf{k}_2$). We then have $\mathbf{k}_3 = -\mathbf{k}_1 - \mathbf{k}_2$ because of translational invariance. The term $\sim k_{2\|}$ then drops out of eq. (4.5), and the quantity $\{...\}$ becomes $k_{1\|}S(\mathbf{k}_2)\{S(\mathbf{k}_3) - S(\mathbf{k}_1)\}$. Finally, we integrate over $k_{2\perp}$, so that G is a function only of $k_{1\|}$; in the following, we will refer to this restricted $G(\mathbf{k}_1, \mathbf{k}_2, \mathbf{k}_3)$ as $g(k)$.

In fig. 4.1 we show $g(k)$ as a function of T (all temperatures are in units of the Onsager temperature) for several system sizes, and $k = 2\pi/L$. The rates are the same as in sec. 2.1, in fig. 4.1 $E = 1.25 \times 4J$. As expected, the Reg is zero apart from fluctuations. The Im$g < 0$ for all T, with a pronounced dip around T_c. The dip is related to the violation of the fluctuation-dissipation theorem, which is maximal at T_c, and for $d = 2$ is predicted to diverge as $1/k$ with increasing system size. Here, $k = 2\pi/L$, and we see the dip amplitude increase with L.

In figs. 4.2 and 4.3 we examine the behavior of $g(k)$ for various E in 40×40 systems. Again, we see that the Re$g = 0$ independent of E. The behavior of Img is somewhat puzzling, however. At larger values of E we see behavior as before, with Im$g < 0$ and a dip corresponding to T_c. On the basis of eq. [38] we expect Img to be proportional to E, though the data suggest no such dependence. (The three minima overlap within the variations seen between runs.) One should note, however, that the quantity which enters eq. (4.5)

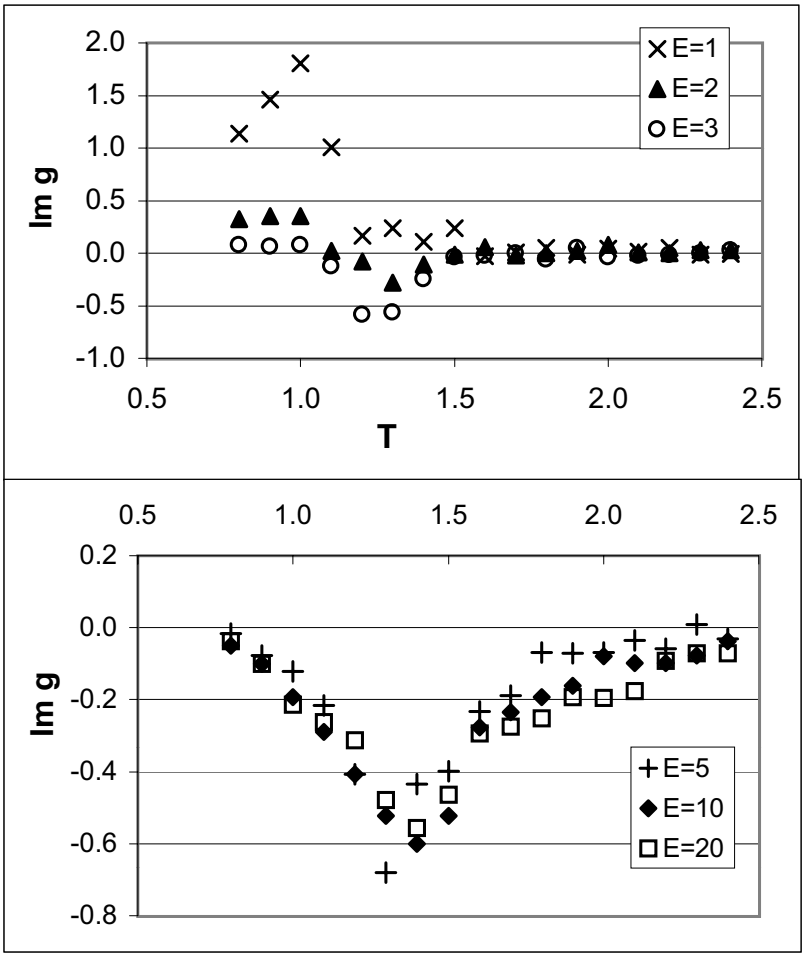

Figure 4.3: Img as a function of T for various E.

is the coarse-grained bias, $\mathcal{E}$, which is really some unknown function of the microscopic parameters, E, J, and T. Indeed, we expect that $\mathcal{E}$ saturates as a function of increasing E. It may be that at the values of E shown in fig. 4.3 this saturation has already occurred.

The data for small E displays some rather unexpected features, namely positive values for Img at low T. Though the theory presented above predicts only $G < 0$, it is crucial to note that this approximation is strictly applicable only for $T \geq T_c$. In particular, G has been calculated *to first order in* $\mathcal{E}$, and we have not considered the effect of the dangerously irrelevant operator u which is necessary for stability of the ordered phase[24]. A more appropriate calculation would set up a perturbation theory around the inhomogenous state, in order to account for the spontaneously broken symmetry. It should

also be noted that the positive part of Img is increasing with decreasing E. At large values of E, the interface is observed to be quite smooth, though a theoretical understanding of how the bias suppresses interfacial roughness is lacking[40]. Of course, at $E = 0$ we are studying the equilibrium Ising model, where the interface is known to undergo a roughening transition[41]. Though G is of course identically zero in the Ising model, it may be that at small E we are observing a complicated crossover from the KLS behavior to the equilibrium behavior. At present, we cannot resolve this issue, and must leave it to further research.

4.3 Summary

We have presented simulation results for the three point correlation function, $g(k)$. This quantity is particularly sensitive to the breaking of reflection symmetry, which results from the uniform hopping bias. A nontrivial $g(k)$ therefore signals the importance of the driving field, and ought to provide a sensitive probe of nonequilibrium behavior. At large E we find behavior which is consistent with theoretical predictions, namely Re$g = 0$ and Im$g < 0$, with a dip in Img at T_c which increases in amplitude with system size. Some puzzles remain for small E however, where Im$g > 0$ at low T. As discussed above, the theoretical treatment is not relevant for the ordered phase. In the future it would be quite interesting to develop perbturbative results for the ordered phase, and try to understand the origin of this behavior.

On a different note, we mention another interesting possibility raised by the nontrivial behavior of the three-point function. More than 20 years ago, Binder developed a powerful computational method to extract critical behavior from finite lattices[35]. The idea is to examine the behavior of the 4^{th} order cumulant as a function of system size, since this particular ratio of moments is essentially the coupling associated with the ϕ^4 term in the LGW Hamiltonian. Using this method one can, for example, estimate T_c *without* any assumptions regarding critical exponents. Of course, for the KLS model in $d = 2$, the ϕ^4 coupling is only dangerously irrelevant, and so the 4^{th} order cumulant method should not be able to give any information. (See, however, the discussion in sec. 2.2.1) Instead, the most relevant nonlinearity is $\mathcal{E}\partial\phi^2$, coming from the bias field and leading to the nontrivial three-point functions discussed in this section[24]. This suggests that a similar analysis

could be carried out by considering the behavior of a 3^{rd} *order cumulant*. Construction of such a quantity remains elusive; it would be a combination of not only correlation functions, but response functions as well. Presumably, in order to measure such a quantity in simulations, it would be necessary to develop a method measure such response functions. Surely, this would be a difficult and interesting project.

Chapter 5

Conclusions and Outlook

In the preceding pages, we have discussed the phase diagram of an interacting lattice gas, driven far from equilibrium. In chapter 2 we presented a detailed Monte Carlo investigation of the phase diagram. Three phases were found, with a homogenous phase at high temperatures and two distinct ordered phases at lower temperatures. Which ordered phase is observed depends on the parameter f, which controls the ratio of the two types of particles. At small f, there is nearly a single species, and a transition is observed into a KLS-type ordered phase. At larger f, the minority species are sufficiently dense to form a transverse blockage, and a sequence of two transitions is observed as the temperature is lowered. First, a continuous boundary is observed into an SHZ-type ordered phase, then at lower temperature a first-order boundary is crossed into the KLS-type ordered phase. At some critical value of f is a bicritical point, where the first-order line branches from the two continuous boundaries.

We investigated the size-dependence of the boundaries in section 2.2.1. We found that the behavior of the continuous transition from the homogenous phase into the SHZ-phase is consistent with the mean-field picture[27], despite the presence of nearest-neighbor attractive interactions and the presence of critical fluctuations. We also found that the bicritical point coincides in the *finite* systems studied with a *single row* of the minority species, independent of system size or geometry. If such scaling holds in the limit of infinite volume, it implies that the SHZ order appears at any finite density of the minority species. This intriguing suggestion indicates a promising line of further inquiry, namely a detailed study of the KLS (single-species) model

in the presence of disorder. The field-theory for the KLS model is well-established[24], with predicted exponents which match rigorous numerical simulations[21],[22],[23]. One could therefore consider whether the couplings associated with disorder are relevant, with the established results guiding theoretical inquiry and simulation studies. There are very few works which consider *nonequilibrium* phase transitions in the presence of disorder[42] [1], and therefore there are no 'rules of thumb' (like the Harris criterion[43]) which inform investigations of equilibrium critical phenomena. Such an investigation would therefore be interesting to a wider audience, as it considers a general question regarding phase transitions far from equilibrium.

We also made use of the established numerical techniques for the KLS model in order to look in some detail at the KLS transition at *finite* E. Previous investigations focussed almost exclusively on the KLS transition at saturation E, here the transition at finite E appears as the $f = 0$ point in our phase diagram. We find that the scaling of the order parameter at finite E is consistent with the established results, and therefore is consistent with the KLS universality class. However, one subtle point begs further investigation. The field theory predicts that all transverse fluctuations are Gaussian, even at T_c. The celebrated Binder cumulant intersection method[35], which uses the crossing of the 4^{th}-order cumulant to extract T_c and the *universal* value for the 4^{th}-order coupling, should therefore fail for the KLS model. In other words, there is no nontrivial fixed point associated with the 4^{th}-order coupling[24]. Unaware of the implications for the Binder method, we used it anyway, and found a remarkably precise crossing at finite E. As we did not observe a unique crossing in our data for saturation E, we speculate that the behavior may be a result of the proximity of the $(E = 0)$ Ising critical point. Indeed, compared to the interparticle interaction strength, the hopping bias is quite small. If this is the case, very precise numerical results will be needed to settle the question. Our data are not sufficiently to resolve the issue, so we must leave it to future investigation.

In chapter 3 we considered the behavior of long-range correlations in the homogenous phase. In both the KLS and the SHZ models, long-range correlations are observed despite the local nature of the dynamics and interactions, though the nature of those correlations is distinct in each case. In our model we are able to move from KLS to SHZ behavior by tuning f. We there-

[1] We have in mind *modification* of phase transitions which are observed in the pure system, and not transitions driven by the presence of disorder.

fore looked for some signal of the two models in the homogenous phase. We developed linearized equations of motion for the coarse-grained particle and charge densities, modelling the fast degrees of freedom as a conserved noise. In order to simplify calculation of the structure factors, we assumed that the two densities experience the *same* noises. Under this assumption, we were able to fit the theoretical results to the experimental data when equal numbers of each type of particle were present (that is, when the average charge density is zero.) However, the data were not so accommodating when we considered nonzero charge density. It would be interesting to attempt to fit the data for nonzero charge density, relaxing the assumption regarding the noise symmetry. This will introduce additional parameters into the fit, and it would therefore be essential to conduct a more systematic search of the parameter space, and quantitatively evaluate the quality of the fit in order to make rigorous comparisons.

In chapter 4, we considered an interesting feature of the KLS model, namely the presence of nonvanishing three-point correlations. These correlations are a direct result of the hopping bias, E, which breaks the inversion symmetry that is present in the equilibrium Ising model. Such correlations may therefore offer a sensitive probe of the nonequilibrium effects of E. In order to extend earlier work, we considered size-dependence of three-point correlations, and also considered the E dependence of the correlations. In our investigations of the E dependence, we found that the measured correlations apparently saturate at modest ($E = 5.0$) values of the hopping bias. Unanticipated features were observed at smaller values of E, where the ordered phase displayed positive three-point correlations. As the existing theory is only useful for $T > T_c$, we cannot speculate on the origin of this behavior. Clearly, if we wish to use the three-point correlations to study the approach to equilibrium theory, we need to develop perturbative results around the ordered phase as well.

A particularly powerful way to use the three-point correlations to probe the nonequilibrium behavior would be to develop a quantity analagous to the Binder method, based on the three-point correlations and response functions. Since the most relevant nonlinearity in the field theory for the KLS model is associated with the hopping bias, and couples to *three* fields, it should be possible to directly probe the fixed point behavior of this coupling. However, unlike in the 4^{th}-order cumulant case discussed above, this quantity would be a combination of both correlation and response functions. Measuring such response functions poses an interesting challenge to the architect of

simulations. In equilibrium, one simply measure a correlation function (say, of fluctuations of the internal energy) and then uses the FDT to compute the corresponding response function (specific heat.) Away from equilibrium, we cannot rely on such correspondences, and must directly measure the response functions.

It is clear that many interesting questions remain. We hope that we have convinced the reader that this is the case, and that future generations will take up these questions in their own work.

Bibliography

[1] S. Katz, J.L. Lebowitz and H. Spohn, *Phys. Rev.* **B28**, 1655 (1983) and J. Stat. Phys. **34**, 497 (1984).

[2] B. Schmittmann, K. Hwang and R.K.P. Zia, *Europhys. Lett.* **19**, 19 (1992).

[3] Ludwig Boltzmann, *Lectures on Gas Theory* (University of California Press, Los Angeles 1964).

[4] E. Ising, *Z. Physik* **31**, 253 (1925).

[5] S. Brush, *Rev. Mod. Phys.* **39**, 883 (1967).

[6] M. Henkel, *Conformal Invariance and Critical Phenomena* (Springer, Berlin 1999).

[7] R.K. Pathria, *Statistical Mechanics,* 2nd ed. (Butterworth-Heinemann, Oxford 1996).

[8] David Mukamel: In: *Soft and Fragile Matter*, ed by M.E. Cates and M.R. Evans (IOP publishing, Bristol 2000).

[9] D.P. Landau and K. Binder, *A Guide to Monte Carlo Simulations in Statistical Physics* (Cambridge U. Press, Cambridge, 2000).

[10] P.A. Rikvold and M. Kolesik, *Phys. Rev.* **E67**, 066113 (2003), P.A. Rikvold and M. Kolesik, *J. Phys.* **A35**, L117-L123 (2002), W. Kwak, D.P. Landau, and B. Schmittmann, in preparation.

[11] P.C. Hohenberg and B.I. Halperin, *Rev. Mod. Phys.* **49**, 435-479 (1977).

[12] G. Grinstein, C. Jayaprakash, and Y. He, *Phys. Rev. Lett.* **55** (2527), B. Schmittmann and F. Schmüser, *Phys. Rev.* **E66** (2002).

[13] H. Hinrichsen, *Adv. Phys.* **49**, 815-958 (2000).

[14] Gunter M. Schutz: In: *Phase Transitions and Critical Phenomena*, vol 19, ed by C. Domb, J.L. Lebowitz (Academic, London 2000)

[15] F. Spitzer, *Adv. Math.* **5**, 247 (1970).

[16] G. Schutz and E. Domany, *J. Stat. Phys.* **72**, 277 (1993).

[17] L.B. Shaw, R.K.P. Zia, and K.H. Lee, *Phys. Rev.* **E68**, 021910 (2003).

[18] P.F. Arndt, T. Heinzel, and V. Rittenberg, *J. Stat. Phys.* **97**, 1 (1999); P.F. Arndt and V. Rittenberg, *J. Stat. Phys.* **107**, 989 (2002).

[19] G. Korniss, B. Schmittmann, and R.K.P. Zia, *Europhys. Lett.* **45**, 431 (1999), J.T. Mettetal, B. Schmittmann, and R.K.P. Zia, *Europhys. Lett.* **58**, 653 (2002), B. Schmittmann, J.T. Mettetal, and R.K.P. Zia: To appear in: *Computer Simulation Studies in Condensed Matter Physics XVI*, ed by D.P. Landau, S.P. Lewis, and H.-B. Schüttler (Springer, Heidelberg 2003).

[20] Y. Kafri, E. Levine, D. Mukamel, G.M. Schutz, and J. Torok, *Phys. Rev. Lett.* **89**, 035702 (2002).

[21] S. Caracciolo, A. Gambassi, M. Gubinelli, A. Pelissetto cond-mat/0106221.

[22] K-t. Leung, Phys. Rev. Lett. **66**, 453 (1991) and Int. J. Mod. Phys. **C3**, 367 (1992).

[23] J-S. Wang, J. Stat. Phys. **82**, 1409 (1996); K-t. Leung and J-S. Wang, Int. J. Mod. Phys. **C10**, 853(1999).

[24] H.K. Janssen and B. Schmittmann, Z. Phys. B **64**, 503 (1986); K-t. Leung and J.L. Cardy, J. Stat. Phys. **44** 567 and **45**, 1087 (1986) (erratum).

[25] B. Schmittmann, H.K. Janssen, U.C. Täuber, R.K.P. Zia, K.-t. Leung and J.L. Cardy, Phys. Rev. **E61**, 5977 (2000).

[26] M.Q. Zhang, J-S. Wang, J.L. Lebowitz and J.L. Vallès, J. Stat. Phys. **52**, 1461 (1988); P.L. Garrido, J.L. Lebowitz, C. Maes and H. Spohn, Phys. Rev. A**42**, 1954 (1990); G. Grinstein, J. Appl. Phys. **69**, 5441 (1991); B. Schmittmann and R.K.P. Zia, J. Stat. Phys. **91**, 525 (1998).

[27] K-t. Leung and R.K.P. Zia, *Phys. Rev.* **E56**, 308(1997).

[28] I. Vilfan, R.K.P. Zia and B. Schmittmann, *Phys. Rev. Lett.* **73**, 2071 (1994).

[29] G. Korniss, B. Schmittmann and R.K.P. Zia, *Europhys. Lett.* **32**, 49 (1995) and *J. Stat. Phys.* **86**, 721 (1996).

[30] K.E. Bassler, B. Schmittmann and R.K.P. Zia, *Europhys. Lett.* **24**, 115 (1993).

[31] G. Korniss, B. Schmittmann and R.K.P. Zia, *Physica* **A239**, 111 (1997).

[32] B. Schmittmann, R.K.P. Zia: In: *Phase Transitions and Critical Phenomena*, vol 17, ed by C. Domb, J.L. Lebowitz (Academic, London 1995)

[33] N. Metropolis, A.W. Rosenbluth, M.M. Rosenbluth, A.H. Teller and E. Teller, *J. Chem. Phys.* **21**, 1087 (1953).

[34] Edward Lyman and B. Schmittmann: To appear in: *Recent Developments in Simulation Studies in Condensed Matter Physics*, vol XVI, ed by D.P. Landau, S.P. Lewis, H.-B. Schüttler, (Springer, Heidelberg 2003)

[35] K. Binder, *Phys. Rev. Lett.* **47**, 693 (1981).

[36] K.-t. Leung, *Phys. Rev. Lett.* **73**, 2386 (1994).

[37] G. Korniss, Ph.D. Dissertation, Virginia Polytechnic and State Institution,(1997, unpublished).

[38] K. Hwang, B. Schmittmann, and R.K.P. Zia, *Phys. Rev.* **E48**, 800 (1993), K. Hwang, B. Schmittmann, R.K.P. Zia, *Phys. Rev. Lett.* **67**, 326 (1991).

[39] P.C. Martin, E.D. Siggia, H.H. Rose, *Phys. Rev.* **A8**, 423 (1973).

[40] K.-t. Leung, K.K. Mon, J.L. Valles, and R.K.P. Zia, *Phys. Rev. Lett.* **61**, 1744 (1988) and *Phys. Rev.* **B39**, 9312 (1989).

[41] H. van Beijeren and I. Nolden, *Structure and Dynamics of Surfaces II*,in: *Topics in Current Physics*, vol. 43 ed. by W. Schommers and P. von Blackenhagen (Springer, Berlin 1987).

[42] B. Schmittmann and K.E. Bassler, *Phys. Rev. Lett.* **77**, 3581(1996), K.B. Lauritsen and H.C. Fogedby, *Phys. Rev.* **E47**, 1563(1992), V. Becker, and H.K. Janssen, *Europhys. Lett.* **19**, 13(1992).

[43] A.B. Harris, *J. Phys.* **C7**, 1671(1974).

Appendix A

Source Code

```
/*-------------------------------------------------------------------------
Sample input file:

2.0                     Drive Strength
.8                      Initial Temperature
.1                      temp interval
.8                      end temp
0                       # neg charges
-6589                   inputseed
1.0                     interaction strength (J)
r                       vertical, horizontal, or random initial configuration
0                       0 for to output config averages, 1 for timetrace
1000                    total MCS...
0                       discard initial MCS
1001                    interval in MCS
threept_multitest       output file name
-------------------------------------------------------------------------*/

#include <string.h>
#include <math.h>
#include <iostream.h>
#include <fstream.h>
#include <iomanip.h>
#include <stdlib.h>
```

```
const int pop = 800; //total population
const int LX = 40;
const int LY = 40; //dimension of square lattice
const int C = 6; //dimension of structure factorarray
const double PI=3.141592653589;
typedef int Grid[LY][LX]; //shorthand for the lattice
typedef double Struct_Array [C][C]; //array of structure
//factors
enum Bond {HORIZONTAL, VERTICAL}; //declaration of bond types

void swap(int&, int&);
void initialize(Grid, int, long*, char);
float ran2(long *idum);
void picture(Grid, ofstream&);
void updatedata(Grid, Struct_Array, Struct_Array,
double&, double&, double&, double&);

void header(ofstream&, int&);

void seed_ran2(long *idum);
void writedata(double, double, Struct_Array, double, double, double, ofstream&);
void average(Struct_Array, Struct_Array,
        Struct_Array, Struct_Array, double, double,
double, double, double&, double&, double&, double&, int);
int main(int NumArgs, char** Argument)

{
Grid lattice;
double E; //drive strength
double T, init_temp, final_temp, temp_int; //temperature
int fracneg; //number of neg charges
long inputseed; //random number generator seed
//seed_ran2(&seed);
double J; //interaction strength
int n1, n2, n3, m1, m2, m3, a, b; //neighbor variables
int numdata = 0;
Struct_Array S;
```

```
Struct_Array N;
Struct_Array STOT ;
Struct_Array NTOT ;
Struct_Array S_AVG;
Struct_Array N_AVG;
double s_sqr10, s_sqr01,//square of
n_sqr10, n_sqr01,
n_sqr01_avg, s_sqr01_avg,
n_sqr10_avg, s_sqr10_avg; //structure factors
double fluc_n01, fluc_n10,
fluc_s01, fluc_s10; //fluctuations
double current = 0.0, avgcurrent = 0.0, jsqr = 0.0, avgjsqr = 0.0, currentfluc;
char config;
int totSteps, discard, interval;
int timetrace; //1 or 0 for timetrace or no timetrace, respectively
int header_on = 1;//allows labels to be printed for timetrace output




double deltaH, prob;

char InFileName[30], OutFileName[30];
char dummyline[132];

if (NumArgs == 1) //Asks for input name if it's not on the
{ //command line
cout << "Enter input file name: ";
cin >> InFileName;
}

else if (NumArgs == 2)
{
// Get the name of the input file from the commmand line
strcpy(InFileName, Argument[1]);

if (!strcmp(InFileName,"?"))
{
```

```
 cout << "Syntax: mutprob [input filename (optional)]''<<endl;
 return 0;
}
}


else
{
cout << "Syntax: mutprob [input filename (optional)]''<<endl;
return 0;
}


ifstream Readfile; //open the input file
Readfile.open(InFileName);
if (!Readfile) //stops the program if there is no
{ //input file
cout << endl << "Input file not found" << endl;
return 0;
}

Readfile >> E; //read in field strength from InfileName
Readfile.getline(dummyline, 132);

Readfile >> init_temp; //Read in T
Readfile.getline(dummyline, 132);

Readfile >> temp_int;
Readfile.getline(dummyline, 132);

Readfile >> final_temp;
Readfile.getline(dummyline, 132);

T = init_temp;

Readfile >> fracneg; //Read in fraction of negative charges
Readfile.getline(dummyline, 132);
```

```
Readfile >> inputseed; //Read in seed for random number generator
Readfile.getline(dummyline, 132);

long* seed = &inputseed;
int inseed = inputseed;


Readfile >> J;
Readfile.getline(dummyline, 132);

Readfile >> config;
Readfile.getline(dummyline, 132);

Readfile >> timetrace;
Readfile.getline(dummyline, 132);

Readfile >> totSteps;
Readfile.getline(dummyline, 132);

Readfile >> discard;
Readfile.getline(dummyline, 132);

Readfile >> interval;
Readfile.getline(dummyline, 132);

Readfile >>  OutFileName; //Read in the name of the output file
Readfile.getline(dummyline, 132);

cout <<endl<<"Output file: "<<OutFileName<<endl;

Readfile.close(); //close the input file

ofstream Writefile; //declare output operator
Writefile.open(OutFileName); //open output file
if (!Writefile)
{
cout << "Ouput file not found"<<endl;
return 0;
```

```
}
cout << endl<<"Output file: "<<OutFileName<<endl;

Writefile << "E = "<< E << endl;
Writefile << "T start = "<< init_temp << endl;
Writefile << "T interval = "<<temp_int<< endl;
Writefile << "T end = " <<final_temp<<endl;
Writefile << "Number of negative charges = "<< fracneg <<endl;
Writefile << "seed = "<<inputseed<<endl;
Writefile << "J = "<<J<<endl;
Writefile <<" total population = "<<pop<<endl;
Writefile <<"Lx = "<<LX<<endl;
Writefile <<"Ly = "<<LY<<endl;
Writefile <<"Total MCS= "<<totSteps<<endl;
Writefile <<discard<<" MCS discarded"<<endl;
Writefile <<interval<<" MCS between measurements"<<endl<<endl;

for(T = init_temp; T<=final_temp;)
{

numdata = 0;
for (int i=0;i<C;i++)
for(int j=0;j<C;j++)
STOT[i][j] = NTOT[i][j] = S_AVG[i][j] = N_AVG[i][j] = 0.0;

fluc_n01 = 0.0;
fluc_n10 = 0.0;
fluc_s01 = 0.0;
fluc_s10 = 0.0;
n_sqr01_avg = n_sqr10_avg = s_sqr01_avg = s_sqr10_avg
= n_sqr01 = n_sqr10 = s_sqr10 = s_sqr10 = 0.0;
avgcurrent = 0.0, jsqr = 0.0, avgjsqr = 0.0, currentfluc = 0.0;


double T_Ons = T*2.269; //convert into units of Onsager temperature

initialize(lattice, fracneg, seed, config);
```

```
for (int MCS=0; MCS<totSteps; MCS++)
{
  current = 0.0;
for (int k=0; k<2*LX*LY; k++) //One MCS
{
int rand = (int(2*LX*LY*ran2(seed)));
//generates a random number between 0 and 3200

Bond type;


if (rand < LX*LY) //bonds numbered 0 thru 1600 are
{
type = HORIZONTAL; //horizontal, start in upper
  //left corner
}
else
{
type = VERTICAL; //vertical bonds are
rand -= LX*LY; //numbered 0 thru -1600

}

int y = abs(rand)/LX;  //y coordinate
int x = abs(rand)%LX;  //x coordinate


if (type == HORIZONTAL)
{
int xR, ydown, yup, x2R, xL;
if (x == (LX-1)) //determines x coord of particle
xR = 0; //immediately right of
else //particle at (x,y)
xR = (x+1); //with PBC

a = abs(lattice[y][x]);  // magnitude of sites
b = abs(lattice[y][xR]); //under comparison
```

```
if (a != b)
{ //no need to continue if we have two
//part. (since exchanges aren't allowed

if (y == 0) //y coordinates of row
ydown = (LY-1);//below
else
ydown = (y-1);
if (y == (LY-1)) //y coord of row above
yup = 0;
else
yup = (y+1);
if (xR == (LX-1)) //x coord of far right
x2R = 0; //neighbor
else
x2R = (xR + 1);
if (x ==0) //x coord of far left
xL =(LX-1); //column
else
xL = (x-1);



n1 = abs(lattice[yup][x]); //coordinates of
n2 = abs(lattice[ydown][x]); //neighbors
n3 = abs(lattice[y][xL]);
m1 = abs(lattice[yup][xR]);
m2 = abs(lattice[ydown][xR]);
m3 = abs(lattice[y][x2R]);




int neighbors_left = n1 + n2 + n3; // sums neighbors
int neighbors_right = m1 + m2 + m3;//for left and right positions
```

```
if (a == 1) //if particle is on the left
{
deltaH = -4*J*(neighbors_right-neighbors_left);
prob = exp(-deltaH/T_Ons);

if (prob >= 1.0)
swap(lattice[y][x], lattice[y][xR]);
else if (ran2(seed) < prob)
swap(lattice[y][x], lattice[y][xR]);
//interchanges the neighbors if 1) it is
//energetically favorable or 2) if a random number
//is rolled smaller than exp(-beta*delatH)

}

else //if particle is on the right
{
deltaH = -4.0*J*(neighbors_left-neighbors_right);
prob = exp(-deltaH/T_Ons);

if (prob >= 1.0)
swap(lattice[y][x], lattice[y][xR]);
else if (ran2(seed) < prob)
swap(lattice[y][x], lattice[y][xR]);
}
}
}
else
{
type = VERTICAL;


int yd, y2d, xleft, xright, yu;

if(y==(LY-1))
yd = 0;
else
```

```
yd = (y + 1);

a = abs(lattice[y][x]);
b = abs(lattice[yd][x]);



if (a != b)
{
if(yd==LY-1)
y2d = 0;
else
y2d = (yd + 1);
if (y ==0)
yu = (LY-1);
else
yu = y - 1;
if(x == 0)
xleft = (LX - 1);
else
xleft = (x - 1);
if(x==(LX-1))
xright = 0;
else
xright = (x + 1);

n1 = abs(lattice[y][xleft]);
n2 = abs(lattice[yu][x]);
n3 = abs(lattice[y][xright]);
m1 = abs(lattice[yd][xleft]);
m2 = abs(lattice[y2d][x]);
m3 = abs(lattice[yd][xright]);


int neigh_up = n1 + n2 + n3;
int neigh_down = m1 + m2 + m3;
```

```
if(a == 1)
{
deltaH = -4.0*J*(neigh_down - neigh_up);
prob = exp(-(deltaH-E*lattice[y][x])/T_Ons);


if(prob >= 1.0){
swap(lattice[y][x], lattice[yd][x]);
current += lattice[yd][x];}
else if (ran2(seed) < prob){
swap(lattice[y][x], lattice[yd][x]);
current += lattice[yd][x];}
}
else
{
deltaH = -4.0*J*(neigh_up - neigh_down);
prob = exp(-(deltaH + E*lattice[yd][x])/T_Ons);

if (prob >= 1.0){
swap(lattice[yd][x], lattice[y][x]);
current -= lattice[y][x];}
else if(ran2(seed) < prob){
swap(lattice[yd][x], lattice[y][x]);
current -= lattice[y][x];}
}
}
}


} //end of one MCS

int rem = MCS % interval;
if ((MCS >= discard) && (rem == 0))//checks to see if it's time for
{ //a measurement
updatedata(lattice, S, N, s_sqr10,  s_sqr01, n_sqr10, n_sqr01);//measurement
numdata++;

current = current/LX/LY;
```

```
jsqr = current*current;


if (timetrace == 0)  //if 'timetrace' is set to 0, this
{ //will record running total of structure factors every
//(interval) MCS
for (int i=0; i<C; i++)
for(int j=0; j<C; j++)
{

N_AVG[i][j] = N_AVG[i][j]*(numdata - 1)/numdata + N[i][j]/numdata;
}

n_sqr01_avg = n_sqr01_avg*(numdata - 1)/numdata + n_sqr01/numdata;
n_sqr10_avg = n_sqr10_avg*(numdata - 1)/numdata + n_sqr10/numdata;
;
avgcurrent = avgcurrent*(numdata - 1)/numdata + current/numdata;
avgjsqr = avgjsqr*(numdata - 1)/numdata + jsqr/numdata;




}
}
} //end of simulation evolution

fluc_n01 = n_sqr01_avg - N_AVG[0][1]*N_AVG[0][1];
fluc_n10 = n_sqr10_avg - N_AVG[1][0]*N_AVG[1][0];

currentfluc = avgjsqr - avgcurrent*avgcurrent;

if (header_on ==1)
header(Writefile, header_on);
writedata(avgcurrent, currentfluc, N_AVG, fluc_n01, fluc_n10, T,  Writefile);
//writes out averages of each structure factor
//and fluctuations to a file, indexed by temperature

T  = T + temp_int;
```

```
}



return 0;

}

void initialize(Grid lattice,  int fracneg, long *seed, char config)
{
int x, y;
int numpos = (pop - fracneg);
if (config == 'r') //random config
{
for (int i=0; i<LY; i++)
for(int j=0; j<LX; j++) lattice[i][j]=0;

for (int k=0; k<numpos;)
{
x= int(ran2(seed)*LX);
y= int(ran2(seed)*LY);
if (lattice[y][x] != 1)
{
lattice[y][x] = 1;
k++;
}
}
for (int l=0; l<fracneg;)
{
int x= int(ran2(seed)*LX);
int y= int(ran2(seed)*LY);
int mag = abs(lattice[y][x]);
if (mag != 1)
{
lattice[y][x] = -1;
l++;
}
```

```
}
}
else if (config == 'v') //vertical strip of mixed charge
{
for (int i=0; i<LY; i++)
for(int j=0; j<LX; j++) lattice[i][j]=0;

int x, y;
int xmax = (LX/2);
for(x=0; x< xmax; x++)
for(y=0; y<LY;  y++)
lattice[y][x] = 1;

for(int neg=0; neg < fracneg;)
{
x = int(ran2(seed)*xmax);
y = int(ran2(seed)*LY);

if (lattice[y][x] != -1)
{
lattice[y][x] = -1;
neg++;
}
}
}
else if (config == 'h') //horizonta;, charge segregated strip
{
for (int i=0; i<LY; i++)
for (int j=0; j<LX; j++) lattice[i][j] = 0;

int x, y;
int ymax = (LY/2);
for (x=0; x<LX; x++)
for (y=0; y<ymax; y++)
lattice [y][x] = 1;

for (int k=0; k<LX; k++)
lattice[ymax][k] = -1;
```

```
int xmax = fracneg - LX;
y = ymax - 1;
for (int l=0; l<xmax; l++)
lattice[y][l] = -1;
}
}




void swap(int& a, int& b)
{
  int temp=a;
  a=b;
  b=temp;
  return;
}

void picture(Grid lattice, ofstream& Writefile)
{
  for (int i=0; i<LY; i++)
  {
    for (int j=0; j<LX; j++)
{
  if (lattice[i][j]==1)
    Writefile << '+';
  else if(lattice[i][j] == -1)
  Writefile << '-';
  else Writefile << '0';
}
    Writefile << endl;
  }
}
```

```
void header(ofstream& Writefile, int& header_on)
              //writes a row of labels for timetrace output
{

Writefile<<setw(10)<<"T/T_Ons";
Writefile<<setw(15)<<"current";
Writefile<<setw(15)<<"j_fluc";
Writefile<<setw(10)<<"density";
Writefile<<setw(10)<<"N(1,0)";
Writefile<<setw(10)<<"N(0,1)";



Writefile<<setw(12)<<"fluc_N(0,1)"<<setw(12)<<"fluc_N(1,0)"<<endl;

header_on = 0;  //turns off header function
}

void writedata(double current, double currentfluc,
               Struct_Array N_AVG, double fluc_n01,
               double fluc_n10, double T, ofstream& Writefile)
{


Writefile.setf(ios::fixed, ios::floatfield);
Writefile.setf(ios::showpoint);
Writefile<<setprecision(5);

Writefile <<setw(10)<<T;
Writefile <<setw(15)<<current;
Writefile <<setw(15)<<currentfluc;


Writefile<<setw(10)<<N_AVG[0][0];
Writefile<<setw(10)<<N_AVG[1][0];
Writefile<<setw(10)<<N_AVG[0][1];
```

```
Writefile<<setw(12)<<fluc_n01<<setw(12)<<fluc_n10<<endl;

}


void updatedata(Grid lattice, Struct_Array S, Struct_Array N,
double& s_sqr10, double& s_sqr01,
double& n_sqr10, double& n_sqr01)
{
  // F[i][j] is structure factor for k=(i*2*PI/LX, j*2*PI/LY)
  for (int i=0; i<C; i++) //loops through all combinations of
  { //wavenumbers for x and y from 0 to 5
    for (int j=0; j<C; j++)
{
      double k = i*2*PI/LX;
  double p = j*2*PI/LY;
  double sRe=0.0;
  double sIm=0.0;
  double nRe=0.0;
  double nIm=0.0;

  for (int x=0; x<LX; x++) //sums over every site in the lattice
  {
    for (int y=0; y<LY; y++)
{
  double r = k*x+p*y;  //k dot (x, y)
  sRe+=lattice[y][x]*cos(r);
  sIm+=lattice[y][x]*sin(r);

  nRe += abs(lattice[y][x])*cos(r);
  nIm += abs(lattice[y][x])*sin(r);
}
  }
  double s=(sRe*sRe+sIm*sIm)/LX/LY; //structure factor of charge dist
  S[i][j] = s;

  double n= (nRe*nRe + nIm*nIm)/LX/LY; //structure factor of particle dist
  N[i][j] = n;
```

```
  if (i==0 && j==1)
  {
  s_sqr01 = s*s; //records square of structure factor for charge
  n_sqr01 = n*n; //and particle distributions for the y direction
  }
  else if (i==1 && j==0)
  {
  s_sqr10 = s*s; //records square of structure factor for charge
  n_sqr10 = n*n; //and particle distributions for the x direction
  }
}
  }

}

//void seed_ran2(long* idum)
//{ // sets seed for ran2 to -1*system clock
// time(idum);
// *idum *= -1;

//}


/*************************************************************
This function is L'Ecuyer's long period random number generator.
It has a period of about 2.3e18.  Call with idum a negative
integer to initialize; thereafter, do not alter idum between
successive deviates in a sequence.  Returns a uniform random
deviate between 0.0 and 1.0 (endpoints excluded).  The C code
for the function comes from Numerical Recipes in C, 2nd edition.
*************************************************************/

#define IM1 2147483563
#define IM2 2147483399
#define AM (1.0/IM1)
#define IMM1 (IM1-1)
```

```
#define IA1 40014
#define IA2 40692
#define IQ1 53668
#define IQ2 52774
#define IR1 12211
#define IR2 3791
#define NTAB 32
#define NDIV (1+IMM1/NTAB)
#define EPS 1.2e-7
#define RNMX (1.0-EPS)

float ran2(long *idum)
{
  int j;
  long k;
  static long idum2=123456789;
  static long iy=0;
  static long iv[NTAB];
  float temp;

  if (*idum<=0)
  {
    if (-(*idum)<1) *idum=1;
else *idum=-(*idum);
    idum2=(*idum);
for (j=NTAB+7; j>=0; j--)
{
  k=(*idum)/IQ1;
  *idum=IA1*(*idum-k*IQ1)-k*IR1;
  if (*idum<0) *idum+=IM1;
  if (j<NTAB) iv[j]=*idum;
}
iy=iv[0];
  }
  k=(*idum)/IQ1;
  *idum=IA1*(*idum-k*IQ1)-k*IR1;
  if (*idum<0) *idum+=IM1;
  k=idum2/IQ2;
```

```
  idum2=IA2*(idum2-k*IQ2)-k*IR2;
  if (idum2<0) idum2+=IM2;
  j=iy/NDIV;
  iy=iv[j]-idum2;
  iv[j]=*idum;
  if (iy<1) iy+=IMM1;
  if ((temp=AM*iy)>RNMX) return RNMX;
  else return temp;
}
```

Vita

Edward Lyman

Date of Birth:	August 28, 1976
Place of Birth:	Boston, MA
Education:	Fall 1999 to Spring 2004: Ph.D. in Physics, Virginia Tech Fall 1994 to Spring 1998: B.S. in Physics, Pennsylvania State University
Teaching Experience:	Fall 1999 to Spring 2001: Graduate Teaching Assistant, Virginia Tech Physics Department
Research Experience:	Fall 2000 to Spring 2004: Graduate Research Assistant, Virginia Tech Physics Department